Remote Sensing of Environment 275 (2022) 113020

Contents lists available at ScienceDirect

Remote Sensing of Environment

journal homepage: www.elsevier.com/locate/rse

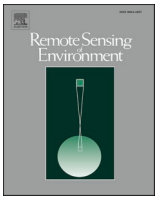

Decadal changes in Arctic Ocean Chlorophyll *a*: Bridging ocean color observations from the 1980s to present time

L. Oziel [a,b,c,*], P. Massicotte [b], M. Babin [b], E. Devred [a]

[a] Ocean and Ecosystem Sciences Division, Fisheries and Oceans Canada, Bedford Institute of Oceanography, Dartmouth, NS B2Y 4A2, Canada
[b] Takuvik Joint International Laboratory, Laval University (Canada) - CNRS (France), Département de biologie et Québec-Océan, Université Laval, Québec, Québec, G1V 0A6, Canada
[c] Alfred-Wegener-Institut Helmholtz-Zentrum für Polar- und Meeresforschung, Am Handelshafen 12, 27570 Bremerhaven, Germany

ARTICLE INFO

Editor: Dr. Menghua Wang

ABSTRACT

Remotely-sensed Ocean color data offer a unique opportunity for studying variations of bio-optical properties which is especially valuable in the Arctic Ocean (AO) where in situ data are sparse. In this study, we re-processed the raw data from the Sea-viewing Wide Field-of-View (SeaWiFS, 1998–2010) and the MODerate resolution Imaging Spectroradiometer (MODIS, 2003–2016) ocean-color sensors to ensure compatibility with the first ocean color sensor, namely, the Coastal Zone Color Scanner (CZCS, 1979–1986). Based on a bio-regional approach, this study assesses the quality of this new homogeneous pan-Arctic Chl *a* dataset, which provides the longest (but non-continuous) ocean color time-series ever produced for the AO (37 years long between 1979 and 2016). We show that despite the temporal gaps between 1986 and 1998 due to the absence of ocean color satellite, the time series is suitable to establish a baseline of phytoplankton biomass for the early 1980s, before sea-ice loss accelerated in the AO. More importantly, it provides the opportunity to quantify decadal changes over the AO revealing for instance the continuous Chl *a* increase in the inflow shelves such as the Barents Sea since the CZCS era.

1. Introduction

The Arctic Ocean (AO) (Fig. 1A) is facing drastic changes due to climate forcing. Among them, the decreases in summer sea-ice extent and volume by about 50% since 1979 (Kwok, 2018; Serreze and Meier, 2019; Stroeve and Notz, 2018) have been identified as major consequences of climate warming. The loss of sea-ice is accompanied by a long list of alterations affecting the whole Ocean-Ice-Atmosphere system of the AO. Understanding how phytoplankton respond to these environmental changes is crucial given their role in the marine ecosystem (Kohlbach et al., 2016), in biogeochemical cycles (Hoppe et al., 2018) and in the biological carbon pump (Lalande et al., 2014; Le Moigne et al., 2015; Mäkelä et al., 2017).

Ocean Color Remote Sensing (OCRS) is a powerful tool to monitor phytoplankton dynamics in the ice-free domain of the AO as it overcomes the lack of in situ observations by providing synoptic time series of chlorophyll *a* concentration (Chl *a*, mg m^{-3}). OCRS has been undeniably at the forefront for monitoring phytoplankton dynamics in the global oceans (McClain, 2009) and has allowed tremendous progress in our understanding of marine ecology (Longhurst et al., 1995), in particular in the AO (Babin et al., 2015). Several studies have already assessed satellite-derived ocean color trends in the AO in terms of Net Primary Production (NPP, Chl *a* based) using either the SeaWiFS (Sea-viewing Wide Field-of-View Sensor, 1997–2010) sensor (Bélanger et al., 2013) the MODIS (MODerate resolution Imaging Spectroradiometer, 2002-ongoing) sensor (Renaut et al., 2018) or a combination of both (Arrigo and van Dijken, 2015; Lewis et al., 2020). These studies concluded that the increase in open-water surface area, duration of the ice-free season and standing stock of phytoplankton were responsible for most of the 57% observed increase in NPP since 1998 (Lewis et al., 2020) along with changes in its phenology (Kahru et al., 2011) and spatial distribution (Oziel et al., 2017; Renaut et al., 2018), in particular in inflow shelves. However, no baseline exists for the standing stocks of biomass and the dynamics of phytoplankton for the early 1980s at the dawn of sea-ice melt acceleration. While Beaulieu et al. (2013) and Henson et al. (2016) recommend a minimum of 30-year time series to derive reliable climate induced biogeochemical changes in the AO, this cannot be currently achieved using "modern-era" satellites only as they

* Corresponding author at: Alfred-Wegener Institute for Polar and Marine Research, Bremerhaven, Germany.
E-mail address: laurent.oziel@awi.de (L. Oziel).

https://doi.org/10.1016/j.rse.2022.113020
Received 17 October 2021; Received in revised form 20 March 2022; Accepted 24 March 2022

span over ~20 years (i.e., SeaWiFS and MODIS).

The goal of the current study is to provide a baseline for phytoplankton biomass for the early 1980s and to quantify decadal changes in Chl *a* to present time in the AO. This study carries on the pioneer work of Gregg and Conkright (2002) and Antoine et al. (2005) who merged CZCS with SeaWiFS at the global scale. We provide the longest time series of climate-compatible AO-adapted satellite-based Chl *a*, an index of phytoplankton biomass identified as an 'Essential Climate Variable' (ECV) for the surface Ocean by the Global Climate Observing System (GCOS). This unique dataset was obtained by combining the data from the first satellite ocean color sensor, the Coastal Zone Color Scanner (CZCS, 1979–1986), with recent data from the SeaWiFS and MODIS sensors (1998–2016). We addressed the issues related to the linkage between CZCS, SeaWiFS and MODIS data, that largely result from technical/instrumental limitations of the CZCS sensor. These limitations include: (1) only four visible spectral bands (443, 520, 550, and 670 nm), (2) a 11-year data gap between the termination of CZCS and the start of the SeaWiFS operations, and (3) a poor spatio-temporal coverage of CZCS due to intermittent operations (i.e., 2 h per day to limit power consumption). In this study, we re-processed the datasets obtained by the recent SeaWiFS and MODIS sensors using methods similar to the ones used for CZCS data in order to achieve coherence, homogeneity and to create a 37-year time series (1979–2016) suitable for climate change studies. We specifically applied the CZCS atmospheric correction procedure and Chl *a* algorithm to the SeaWiFS and MODIS raw data. The results from this challenging re-processing effort are extensively quality-controlled, and interpreted using an innovative bio-regional approach (Fig. 1B) (Spalding et al., 2012). Finally, using the homogenized dataset, we assessed the decadal changes in Chl *a* that occurred in the AO between 1979 and 2016.

2. Data

The CZCS Level-3 binned data at ~4.6-km spatial resolution were downloaded from the NASA distributed Active Archive Center (DAAC) for satellite Ocean Biology (OB) by the Ocean Biology Processing Group (OBPG, https://oceandata.sci.gsfc.nasa.gov/), while the SeaWiFS and the MODIS archives were downloaded in Level-1A format and processed to Chl *a* (see section 3.2). All datasets were re-projected on a sinusoidal ~27.8-km resolution grid. In addition to ocean color data, daily composites of sea-ice concentration data were obtained from the National Snow and Ice Data Center for a grid resolution of 25 km^2 (dataset ID NSIDC-0051, Cavalieri et al., 1996). The dataset provides a consistent time series of sea-ice concentration between 1979 and 2016 obtained from brightness temperatures measured by several passive microwave instruments (SMMR, SSM/I, SSMIS). Cloud fraction between 1979 and 2016 was downloaded from the ERA-Interim model reanalysis made available by the European Centre for Medium-Range Weather Forecasts (ECMWF) from a nominal 79-km (T255) grid spacing (Dee et al., 2011).

3. Methods

3.1. Bio-regionalization of the Arctic Ocean

The first version of the book 'Ecological Geography of the Sea' (Longhurst, 1981) evidenced the response of planktonic ecosystems to regional oceanography. In the second book edition (Longhurst, 2007), the author identified the AO as a specific ecological province (i.e. the 'Boreal Polar Province' BPLR) that belongs to the 'polar' biome together with the Southern Ocean. A more detailed bio-regionalization was undertaken by Spalding et al. (2012) who distinguished 12 realms, 62 provinces and 232 bio-regions in the 'Marine Ecoregions of the World'. The AO was characterized as a specific province made of 27 bio-regions (Fig. 1B). The bio-regions were distinguished based on their geographic, physical and ecosystem properties derived from in situ measurements. The 27 bio-regions are considered as areas of homogeneous species composition, and clearly distinct from adjacent systems. They are also characterized by specific oceanographic and topographic features (e.g. ocean dynamics, sea-ice regimes, bathymetry). The present pan-Arctic study relied on the bio-regional approach of Spalding et al. (2012) in order to account for the bio-optical heterogeneity of the AO allowing a regional characterization of errors and correction of biases between satellites.

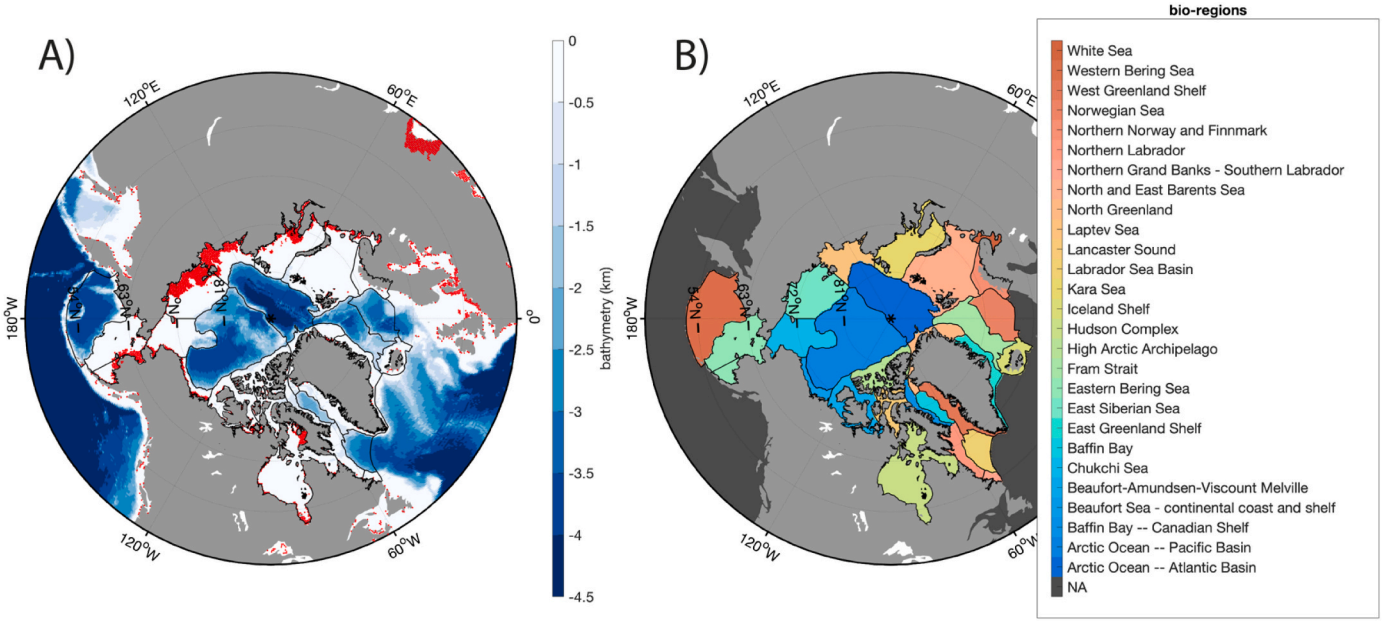

Fig. 1. Arctic Ocean bathymetry and bio-geography. Bathymetry with masked shallow areas (depth < 25 m) in red (A), and the 27 arctic bio-regions (B) from WWF (updated from Spalding et al., 2012). The dataset covers the whole region above 45°N, but the studied area is defined by the arctic colored bio-regions. The black background refers to regions considered outside the AO which are not included in this study. (For interpretation of the references to color in this figure legend, the reader is referred to the web version of this article.)

3.2. 'New' re-processed dataset (NEW)

The processing used for the CZCS dataset has remained unchanged since the R2014.0 re-processing (R2014.0) carried out by the OBPG. This re-processing is similar to the processing applied to modern sensors like SeaWiFS and MODIS, except for specificities in the atmospheric correction procedure and assumptions used to determine the aerosol contribution to the atmospheric signal. CZCS was launched in 1978 as a "proof-of-concept" instrument (Mitchell, 1994) and was not equipped, unlike MODIS and SeaWiFS, with a pair of near infrared (NIR) bands (where water-leaving radiance contribution to the total signal reaching the satellite is very small to null) to determine the aerosol type and radiance contribution to the total top-of-atmosphere signal. Instead, CZCS relies only on a single wavelength at 670 nm (750 nm was not designed for ocean observations) to address atmospheric correction. "CZCS-like" atmospheric correction uses an iteration scheme to account for possible contribution from the ocean to the total signal at the top of the atmosphere at 670 nm. The iteration scheme originally proposed by Bricaud and Morel (1987), was further developed by the OBPG (modified from Stumpf et al., 2003) to include an assumption about the aerosol model that is used to extrapolate the aerosol contribution to the atmospheric signal at shorter visible wavelengths. Note that the same calibration strategy is now applied to all sensors since the R2006.0 re-processing (Franz et al., 2007; Werdell et al., 2007).

The 'CZCS-like' atmospheric correction was applied to SeaWiFS and MODIS Level-1B datasets (see step 1 to 2 in the flowchart in Fig. 2). This correction consisted of processing the entire SeaWiFS and MODIS datasets from all Level-1A source files, to Level-2 files using the same atmospheric correction that was applied to CZCS. This approach further assumes a fixed aerosol model (r70f10, 10% fine mode fraction at 70% relative humidity as in Ahmad et al., 2010). Only pixels located above 45°N were selected. Finally, the resulting Level-2 files were then temporally and spatially binned at the pixel level using averages to obtain merged daily L3 files at a spatial resolution of 4.6 × 4.6-km (step 2 to 3 in Fig. 2).

This re-processing of SeaWiFS and MODIS data provided remote sensing reflectance (Rrs), from which Rrs(443) and Rrs(555) were used to estimate Chl *a* concentration. We used the band-ratio empirical algorithm for oceanic Case 1 waters from Morel and Maritorena (2001) (Morel-3; step 3 to 4 in Fig. 2 and **S1**) following the recommendations of Antoine et al. (2005) who merged CZCS and SeaWiFS datasets for studies at temperate latitudes. This Chl *a* dataset made of data from the three sensors (i.e., CZCS, SeaWiFS and MODIS), with "CZCS-like" atmospheric correction and the empirical Morel-3 Chl *a* algorithm is referred to as the NEW dataset in the manuscript. The re-processing of the SeaWiFS and MODIS raw data required the equivalent of ~10 years of cumulated computing time on one processor (Intel Platinum 8260 Cascade Lake @ 2.4Ghz). NEW was compared with a reference dataset (REF) which represents what was considered one of the most performant dataset for the AO. REF Chl *a* dataset includes SeaWiFS and MODIS and is based on the Garver-Siegel-Maritorena semi-empirical algorithm (GSM01, Maritorena et al., 2002; Maritorena and Siegel, 2005). This algorithm was selected because (1) it was found to perform better than standard empirical algorithms, such as the standard band ratio OC3/4 ocean color algorithm, especially in Arctic waters that are subject to high concentrations of Colored Detrital Matter (CDM) content due to freshwater inputs and resuspension of bottom sediment; (2) semi-analytical models such as GSM01 account for variations in CDM and particle backscatter yielding more accurate surface Chl *a* concentration compared to empirical models (Ben Mustapha et al., 2012); (3) the GSM01 was also found to be associated with the best performing Chl *a* estimations (Brewin et al., 2015) and Chl *a* based primary production models (see models 12–17 in Lee et al., 2015).

3.3. Outliers, data coverage and composite maps calculation

Because the Morel-3 algorithm was developed for non-coastal waters and does not differentiate phytoplankton absorption from detritus or CDOM absorption (unlike the GSM01 algorithm), we masked nearshore areas with depth shallower than 25 m (see red area in Fig. 1A) and Chl *a*

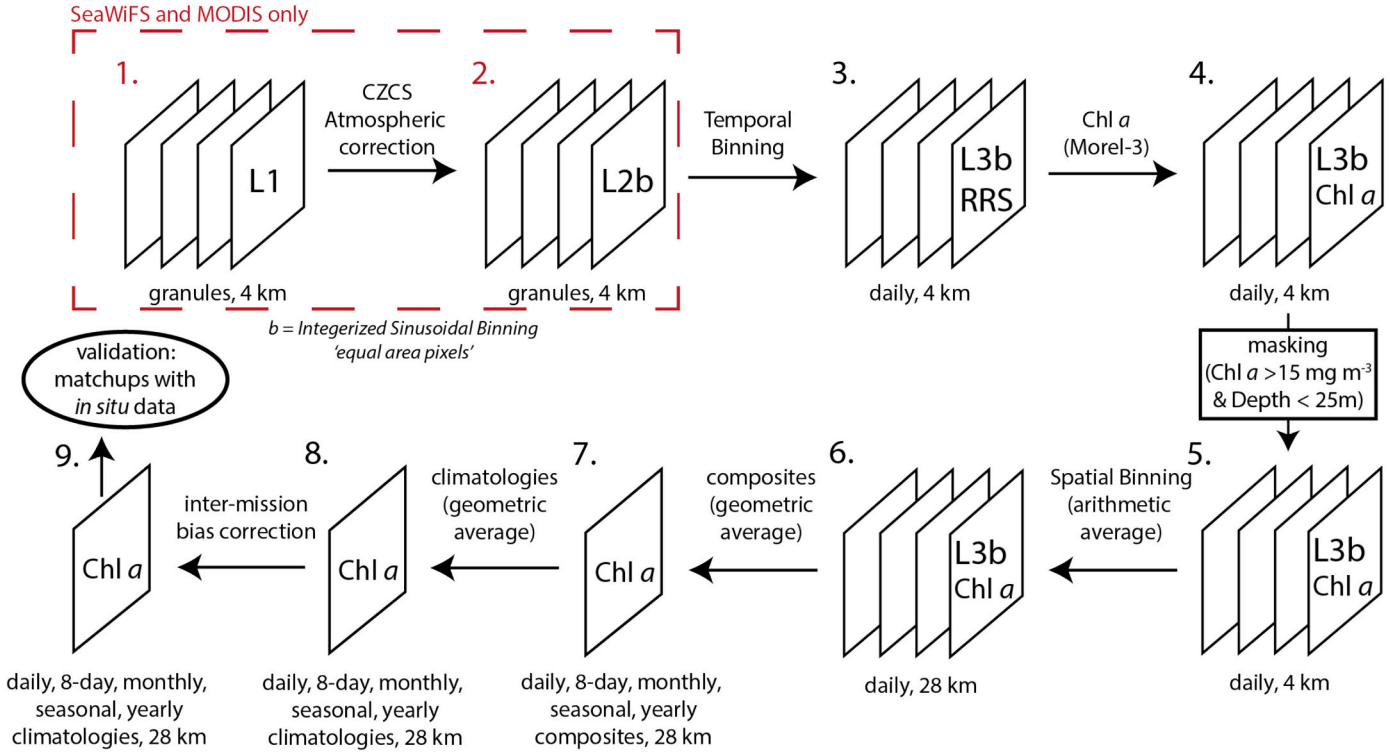

Fig. 2. Schematic view of the data re-processing steps. All steps from 1 to 8 are described in the method section. This re-processing produces the 'NEW' dataset, in opposition with the 'REF' dataset which is our reference 'standard' dataset.

higher than 15 mg m^{-3} (steps 4 to 5 in Fig. 2) in order to minimize pixels located in regions influenced by terrestrial inputs. Indeed, shallow areas are often associated with turbid waters contaminated by yellow substances or sediments especially during summer (Matsuoka et al., 2012; Mitchell, 1992; Ben Mustapha et al., 2012), which artificially increases Chl *a* derived from band ratio. Turbid waters can also cause failure of the atmospheric correction performed in the red-NIR domain. Implementation of these criteria and their impacts on the Chl *a* were further studied in the next section.

Daily maps were binned onto a sinusoidal 27.84-km resolution grid (steps 5 to 6, Fig. 2) and then aggregated into composite maps (steps 6 to 7) at several temporal resolutions: daily, 8-day, monthly, seasonal (April–May-June for spring and July–August-September for summer) and annual (April to September) composites. Any given composite map was computed using the geometric average of all available daily maps covering the period of interest on a pixel-per-pixel basis. Note that the period from October to March was discarded from our analysis due to the absence of data during the polar night and that geometric mean was preferred over the arithmetic mean to minimize the effects of potential remaining outliers. The combination of spatial binning (Fig. 3 AB) and time-averaging (e.g. monthly, Fig. 3C) resulted in a significant increase (by a factor of 10) in the data coverage of the CZCS dataset, making it comparable to the spatial coverage of the SeaWiFS and MODIS datasets.

The existence of temporal gaps in the CZCS time series results from issues in the power demand from the nine sensors onboard the Nimbus-7 platform, which prevented their continuous operations. The CZCS sensor was operated on an intermittent schedule and collected data only two hours per day on average. One should be aware that missing data is an inherent issue when working with satellite ocean color passive sensors (Racault et al., 2014). This problem is especially acute in the Arctic due to a combination of polar night, sea-ice, and cloud cover, and is amplified by the poor spatial coverage of CZCS (Fig. 3C). Racault et al. (2014) showed that when averaged over 8 years for climatological maps, the CZCS data coverage is adequate for climate-related marine studies. However, their study only assessed regions at lower latitudes (< 75°N) where more data were available compared to polar latitudes. We decided to only assess decadal changes, synthesizing the CZCS (1979–1984), SeaWiFS (1998–2006) and MODIS (2007–2016) periods into three climatologies in order to minimize the impacts of missing data (step 7 to 8 in Fig. 2) and the discontinuity in the three time series. Note that the CZCS years 1985 to 1986 were discarded in the current study due to large uncertainties in the sensor calibration, which increased towards the end of its operational life (Antoine et al., 2005; Martinez et al., 2009; Racault et al., 2014). Similarly, SeaWiFS data after 2007

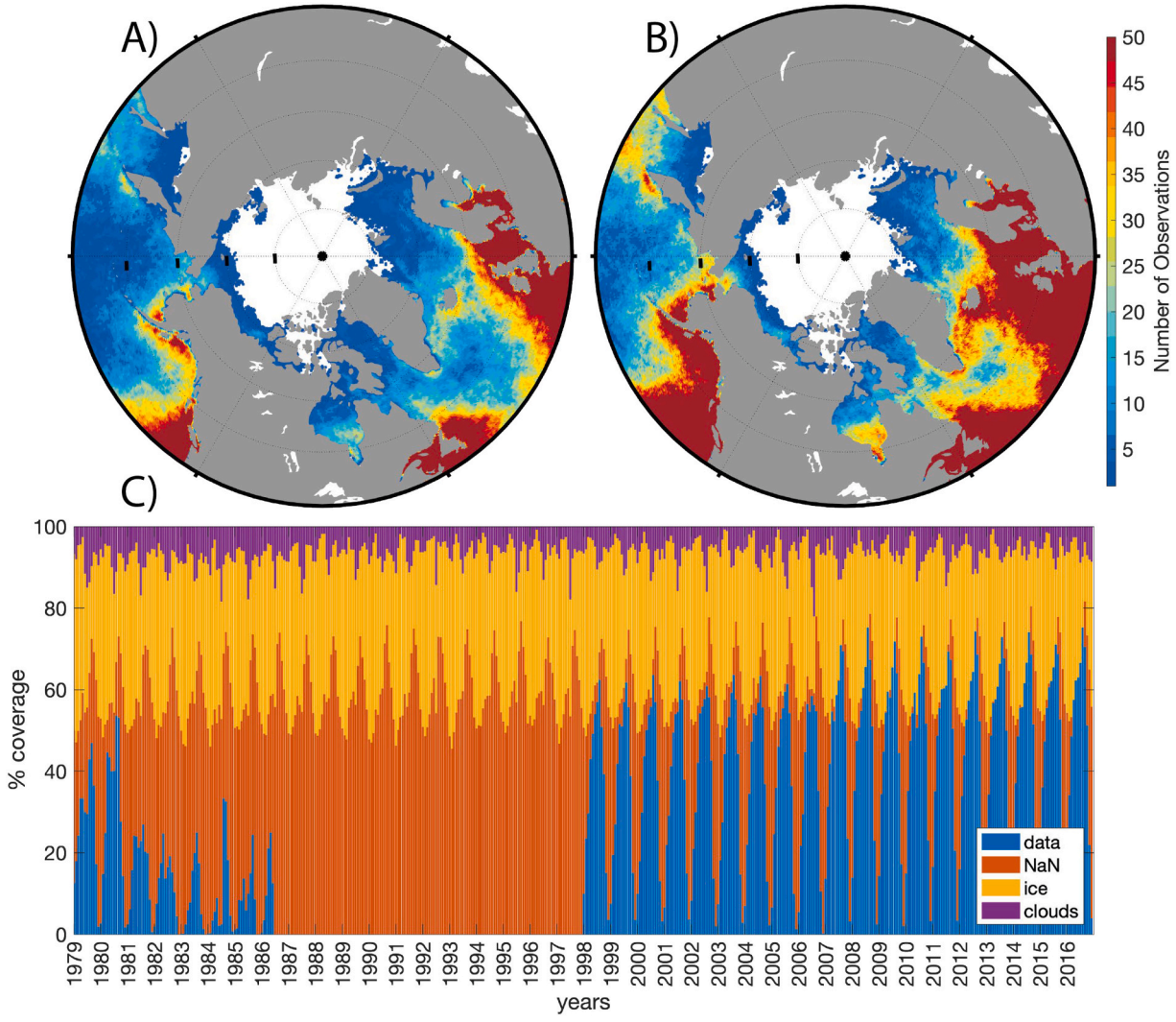

Fig. 3. Spatio-temporal data coverage. CZCS data coverage for daily maps binned onto 4-km (A) and 28-km (B) pixels for the 1979–1984 period. Proportion of ocean color data computed over the AO (CZCS, SeaWiFS and MODIS) prior to sea-ice, clouds or unexplained absence of data (denoted NaN, due to CZCS shut down or other flags) for monthly composite maps at 28-km definition (C). (For interpretation of the references to color in this figure legend, the reader is referred to the web version of this article).

were removed from the study due to large data gaps and persistent temporal calibration drifts despite a correction added in the R2014.0 NASA re-processing (Eplee et al., 2007). One could also argue that MODIS data after 2013 could be discarded due to radiometric degradation (Meister and Franz, 2014). However, we found that it had little impacts on our results (see **Fig. S4**) and decided to keep the data from 2014 to 2016 to increase the data coverage. Note that we also decided not to include data from the Ocean Color and Temperature

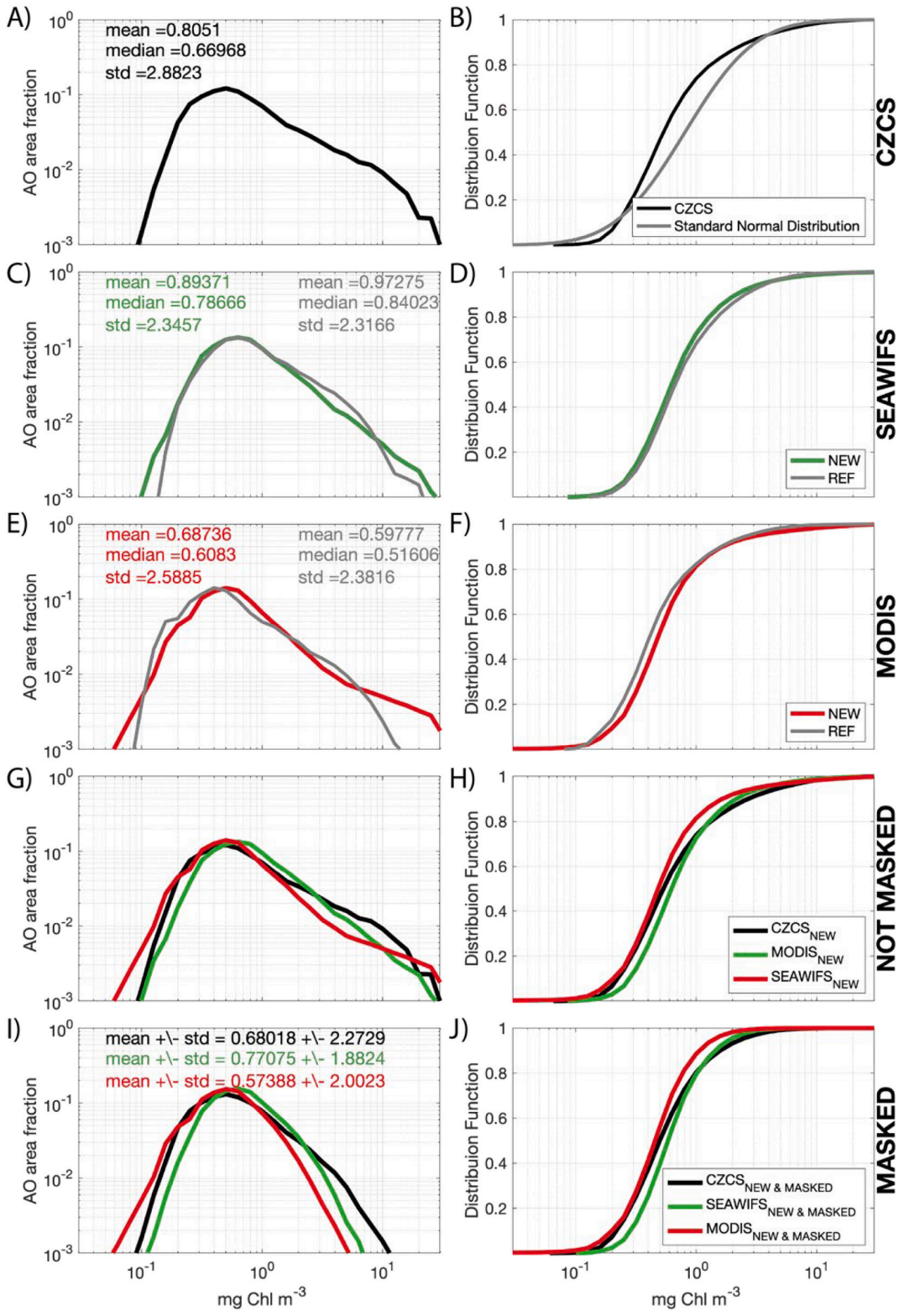

Fig. 4. Frequency distribution (left) and associated cumulative frequency function (right) derived using monthly climatology maps of Chl *a* concentration (mg m^3) from all years in the whole Arctic Ocean. Distributions are calculated for CZCS (A, B), SeaWiFS (C, D) and MODIS (E, F) sensors and for the NEW (re-processed "CZCS-like") datasets (G, H) and masked NEW datasets (I, J). Masked data are data without coastal areas (depths shallower than 25 m) and Chl *a* greater than 15 mg m^{-3}. (For interpretation of the references to color in this figure legend, the reader is referred to the web version of this article).

Scanner (OCTS) which only operated between November 1996 and June 1997 and represented only three valid monthly images for the AO with no overlapping with SeaWiFS.

3.4. Chl *a* log-normal distribution

As shown by Campbell (1995), Chl *a* follows a log-normal (base-10) distribution in the open ocean. We performed both Kolmogorov-Smirnov and Shapiro-Wilks tests to assess the normality of our Chl *a* dataset. The results showed a significant deviation from normality for both the linear and the $\log_{10}$-transformed datasets (p-value <0.001). This result might be explained by the high sensitivity of such tests that account for very small deviations from the normality when dealing with very large sample size ($N \sim 8 \times 10^5$). The Chl *a* log-normal distribution was therefore visually compared to the CZCS Chl *a* distribution (Fig. 4B). We also computed statistics of skewness and kurtosis for annual climatological Chl *a* distribution. For the log-transformed distribution of Chl *a*, skewness and kurtosis ranged typically between −0.46 and 1.89 (CZCS skewness = −0.07, CZCS kurtosis = 1.41, SeaWiFS skewness = −0.46, SeaWiFS kurtosis = 1.89, MODIS skewness = 0.36, MODIS kurtosis = 1.72), which is considered acceptable to prove normal univariate distribution (values are expected to vary between −2 and 2 according to Gravetter and Wallnau 2014). These indicators are respectively up to one order of magnitude higher for the distribution of Chl *a* in the linear space (CZCS skewness = 1.89, CZCS kurtosis = 5.19, SeaWiFS skewness = 2.19, SeaWiFS kurtosis = 6.52, MODIS skewness = 2.20, MODIS kurtosis = 6.61) than for the $\log_{10}$-transformed. Given these results, the Chl *a* dataset was considered to follow a lognormal distribution for this study.

3.5. Statistics for comparison of NEW vs. REF datasets

To evaluate quantitatively the performance of the NEW Chl *a* reprocessing compared with the REF dataset (considered in this study as the reference measurements), a suite of statistical indices were derived as recommended by the Ocean Color Climate Change Initiative (OC-CCI; see Brewin et al., 2015; Evers-King et al., 2017; Sathyendranath et al., 2019).

We computed the following set of statistical indices to assess the quality of the re-processed SeaWiFS and MODIS Chl *a* fields, which were previously $\log_{10}$-transformed. We derived the root-mean-square difference (RMS or Δ, Equ. 1) and bias (δ, Equ. 2) to report on dispersion and offset:

$$\Delta = \left(\frac{1}{N} \sum_{i=1}^{N} \left(log_{10}\left[Chl_{2,i}\right] - log_{10}\left[Chl_{1,i}\right] \right)^2 \right)^{1/2} \quad (1)$$

$$\delta = \frac{1}{N} \sum_{i=1}^{N} \left(log_{10}\left[Chl_{2,i}\right] - log_{10}\left[Chl_{1,i}\right] \right) \quad (2)$$

These indicators were associated with the unbiased root-mean-square (URMS) difference (Δ_u, often referred to as centered Δ, Equ. 3) expressed on a log-10 scale:

$$\Delta_u = \left(\frac{1}{N} \sum_{i=1}^{N} \left(\left(log_{10}\left[Chl_{2,i}\right] - \overline{LC_2} \right) - \left(log_{10}\left[Chl_{1,i}\right] - \overline{LC_1} \right) \right)^2 \right)^{1/2} \quad (3)$$

Where $\overline{LC_k}$ indicates the average of the distributions $(\log(\mathrm{Chl}_{k,i}))_{i=1,N}$ for the dataset k.

A small Δ indicates a small difference in magnitude between two datasets. The Δ coefficient consists of two components: i) δ representing the difference between the means (i.e. offset of the mean) and ii) Δ_u representing the difference in variability (i.e. dispersion around the mean) between two datasets. Thus, bias δ and Δ_u provide measures of how well the mean (i.e. accuracy) and the variability (i.e. precision) are represented and vary in time and/or space. We also calculated the Spearman's correlation coefficient r_s, the slope S and the intercept I of the linear regression between the $\log_{10}$-transformed Chl *a* dataset using a standardized major axis (SMA) type II linear regression. Note that even if a normal distribution is assumed for the $\log_{10}$-transformed Chl *a*, we also derived a non-parametric statistical metric called Mean Absolute Percent Deviation (MAPD in %) applied to untransformed Chl *a* following Werdell et al. (2013) which provided an easily interpretable indicator. MAPD estimates the average difference following the equation:

$$MAPD = 100 \times \frac{1}{N} \sum_{i=1}^{N} \left| \frac{Chl_{2,1} - Chl_{1,i}}{Chl_{1,i}} \right| \quad (4)$$

Calculations were made on the ensemble of N pairs of valid Chl *a* values (NEW vs. REF) from SeaWIFS and/or MODIS composite maps (see section 3.3) for each available year. All statistical indices were also summarized for each specific oceanic bio-region (spatially averaged) if the number of valid pairs were greater than 10% of the maximum number of possible valid pairs (i.e., total number of pixels in a given region).

4. Results: Bridging the re-processed SeaWiFS and MODIS datasets with CZCS

The main objective of applying the "CZCS-like" algorithms to the SeaWiFS and MODIS observations was to achieve compatibility among the datasets from the three sensors. In a first step, we exhaustively verified the quality of the produced dataset to ensure that it was not degraded beyond scientific meaning (e.g. differences >100%, section 4.1). This was achieved by comparing the NEW and the REF (SeaWiFS and MODIS) datasets using the statistical indices described in the previous section. First, we carried out a general comparison at the pan-Arctic scale (section 4.1.1) and second, extended the analysis to bio-regional and seasonal scales (section 4.1.2). We also estimated the inter-mission bias between the NEW SeaWiFS and MODIS datasets based on their overlapping period (2003–2006, section 4.2) and corrected MODIS from possible bias. While the absence of overlap between CZCS and SeaWiFS hinders inter-mission bias correction, it cannot be overlooked. Although the intent of this work was to be as independent as possible from an in situ data collection, we also assessed the inter-mission bias by comparing the NEW dataset (CZCS, SeaWiFS and MODIS) with in situ measurements of Chl *a*, providing an additional quality assessment. Finally, climatological mean and decadal changes are presented in section 4.3. The main outcomes of the section 4 will be discussed in the section 5.

4.1. Assessing the quality of the NEW dataset vs. REF

4.1.1. General results at pan-Arctic scale

The comparison between the entire REF and the NEW datasets for SeaWiFS and MODIS (i.e. all months, all years, all regions) are shown in Fig. 4. Left panels show the distribution of the chlorophyll *a* concentration in terms of the fraction of the AO area covered by concentration bins. Note that the CZCS cumulative distributions displayed in Fig. 4B shows a reasonable agreement with the standard log-normal distributions in gray. The NEW processing does not substantially differ from the REF Chl *a* values for SeaWiFS and MODIS, and the three missions (CZCS in Fig. 4A-B, SeaWiFS in Fig. 4C-D and MODIS in Fig. 4E-F) do have similar Chl *a* concentration averages (0.81, 0.89 and 0.69 mg m^{-3}) and distributions between 0.03 and 30 mg m^{-3} (Fig. 4G-H) when nearshore data are not masked. However, small discrepancies occurred for some large Chl *a* values (i.e., > 2 mg m^{-3}) and are generally attributed to failures of the atmospheric correction or to the Morel-3 algorithm which is not adapted for coastal waters (see section 3.2). After masking pixels (excluding [Chl *a*] > 15 mg m^{-3} and depth < 25 m) to remove possible outliers, the Chl *a* distributions remain similar between sensors

evidencing a fair agreement between missions (0.68, 0.77 and 0.57 mg m^{-3} for CZCS, SeaWiFS and MODIS respectively, Fig. 4I-J) despite the persistence of slight discrepancies for large Chl *a* values (i.e., Chl $a > \sim 5$ mg m^{-3}).

The cumulative distributions showed that Chl *a* concentrations greater than 15 mg m^{-3}, which were masked in the final implementation of the NEW dataset, represented less than 1% of the entire AO surface area independently of the sensor used (Fig. 4H). They also revealed that about 80% of the AO surface area corresponded to mesotrophic waters with moderate Chl *a* (i.e. 0.2 < Chl *a* < 1 mg m^{-3}). The oligotrophic domain (i.e. Chl $a < 0.2$ mg m^{-3}) corresponded to less than 1% and the eutrophic domain (i.e. Chl $a > 1$ mg m^{-3}) corresponded to about 20% of the AO surface area. When superimposed, the cumulative distribution functions from the three different missions are also in very close agreement. Over the entire AO (27 bio-regions, all months, all years) the statistical indices evaluating the performance of NEW against REF showed high correlation coefficients for both SeaWiFS ($S = 1.01$, $I = 0.045$, $r_s = 0.93$, p-value <0.001) and MODIS ($S = 1.01$, $I = 0.026$, $r_s = 0.96$, p-value <0.001). Differences between NEW and REF, expressed in terms of URMS, bias and MADP (%) were also reasonably low for SeaWiFS ($\Delta_u = 7\ 10^{-2}$, $\delta = -3\ 10^{-2}$, MAPD = 18%) and MODIS ($\Delta_u = 4.8\ 10^{-2}$, $\delta = +5.6\ 10^{-2}$, MAPD = 19.8%). The comparison between NEW and REF led to Chl *a* bias of opposite signs for SeaWiFS and MODIS suggesting that NEW underestimates (overestimates) REF for SeaWiFS (MODIS).

4.1.2. Spatio-temporal impacts of the re-processed Chl a fields for SeaWiFS and MODIS

A suite of statistical indices was examined to assess the impacts of the re-processing on the Chl *a* estimation in time (seasonally and annually) and space (bio-regionally) for SeaWiFS and MODIS. Such a detailed description was needed to identify the strength and limitations of the NEW dataset that extends to the CZCS era. Confirmation of the robustness and reliability of the NEW dataset is a necessary step prior to the calculation of long-term differences and the subsequent biological interpretations. For the sake of clarity, we limited the description of the statistical indices to the most striking results for some bio-regions. The reader can refer to the detailed statistical indices for any given bio-region in the supplementary material (statistical indices are presented in **Tables S1** to **S6**, mean climatological values are presented in Table 1).

i) Impacts of the seasonal dynamics on the re-processing quality.

The spatial distributions of r_s, Δ_u, δ and MAPD for SeaWiFS and MODIS revealed seasonal patterns at pan-Arctic scale as illustrated in Fig. 5 (SeaWiFS, 1998–2010) **and 6** (MODIS, 2003–2016). On average, the MAPD remained stable for MODIS (SeaWiFS) over the Arctic with 23% (24%) in spring and 24% (19%) in summer. For both sensors, MAPD remained almost evenly distributed in spring. In summer, however, larger MAPD values occurred in the 'northernmost' areas and along the Russian shelves (Fig. 5K and 6K). For example, the Atlantic basin of the AO (usually also called the Eurasian basin, see Fig. 1) exhibited large MAPD values in spring (60% for SeaWiFS) perhaps due to the small number of available data (very poor data coverage = 2.7%). During the more recent MODIS period, the decrease in sea-ice cover and subsequent increase in data coverage (11.9%) resulted in a better precision and accuracy.

Those differences between the NEW and REF datasets for both SeaWiFS (Fig. 5) and MODIS (Fig. 6) were attributed to both the presence of variability (Δ_u) and bias (δ) in the Chl *a* signal which followed similar seasonal spatial dynamics than the MAPD. The largest differences were found where Chl *a* varied the most, i.e. in the sub-Arctic regions in spring and in the northernmost regions in summer. As an example, in the eastern Bering Sea, precision was lower in spring ($\Delta_u = 0.13$ for SeaWiFS; $\Delta_u = 0.09$, for MODIS) than in summer (JAS; $\Delta_u = 0.12$, for SeaWiFS; $\Delta_u = 0.07$, for MODIS, Fig. 5A-B, 6A-B). The differences between the NEW and REF datasets were also explained by the presence of systematic bias in Chl *a* (δ, see Fig. 5D-E, 6D-E). For example, for SeaWiFS in spring (Fig. 5D), most of the western (Atlantic) sector was characterized by positive δ whereas it was negative almost everywhere else. When averaged over the whole AO, positive and negative δ almost compensated each other to about $-4.5\ 10^{-2}$. The evolution of δ followed a similar seasonal variation than the one for Δ_u, i.e., a poleward decrease in accuracy (increase in δ) from spring to summer. This translated into a decrease in δ at lower latitudes and an increase with large positive δ at the northernmost latitudes in summer, in particular along the sea-ice edge in the Pacific sector and the Russian shelves. For MODIS (Fig. 6E), the whole AO was characterized by a more spatially-homogeneous positive bias ($\delta = 4.6\ 10^{-2}$ in spring; $\delta = 6\ 10^{-2}$ in summer) except for some very local anomalies such as the areas around James Bay south of the Hudson Complex, the Ob and Yenisey river deltas in the Kara Sea, and along the sea-ice edge. In contrast, SeaWiFS was characterized by seasonal negative bias ($\delta = -4.5\ 10^{-2}$ in spring; $\delta = -3.2\ 10^{-2}$ in summer).

ii) Impacts of the spatial variability at bio-regional scale on the re-processing quality.

In addition to the expected large-scale seasonal variations, spatial features were also associated with intrinsic bio-regional specificities (Fig. 1B). Each bio-region has a unique bio-optical signature that results from topographic, local trophic interactions and biogeochemical fluxes such that the quality of the NEW dataset differs among regions. To avoid seasonal effects in the spatial analysis, bio-regional statistical indices

Table 1
Bio-regional annual averaged Chl *a* concentrations in linear scale [mg m^{-3}] for the three periods CZCS (C, 1979–1984), SeaWiFS (S, 1998–2006), MODIS (A, 2007–2016) and respective decadal relative changes SeaWiFS-CZCS ($\Delta_{S\text{-}C}$) and MODIS-SeaWiFS ($\Delta_{A\text{-}S}$) [%]. Note that only bio-regions with more than 50% data coverage for CZCS are shown. The reader can find data coverages for all three sensors in **Table S14**.

Bio-regions	C	S	A	$\Delta_{S\text{-}C}$ [%]	$\Delta_{A\text{-}S}$ [%]	Δ_{TOTAL} [%]
Arctic Ocean – Atlantic Basin	–	1.081	1.812	–	68	68
Arctic Ocean – Pacific Basin	1.105	0.53	0.841	−52	59	7
Baffin Bay – Canadian Shelf	0.907	0.708	0.871	−22	23	1
Beaufort Sea – continental coast and shelf	1.769	2.259	1.808	28	−20	8
Beaufort-Amundsen-Viscount-Melville	1.197	0.585	0.653	−51	12	−39
Chukchi Sea	0.9	1.008	1.053	12	4	16
Baffin Bay	0.686	0.521	0.671	−24	29	5
East Greenland Shelf	1.061	0.771	0.915	−27	19	−8
East Siberian Sea	0.939	1.48	1.922	58	30	88
Eastern Bering Sea	1.152	1.361	1.153	18	−15	3
Fram Strait	0.768	0.738	0.915	−4	24	20
High Arctic Archipelago	0.964	0.856	1.451	−11	70	59
Hudson Complex	1.064	0.903	0.953	−15	6	−9
Iceland Shelf	0.978	1.071	1.122	9	5	14
Kara Sea	0.61	1.434	1.663	135	16	151
Labrador Sea Basin	0.696	0.732	0.77	5	5	10
Lancaster Sound	0.853	0.914	1.106	7	21	28
Laptev Sea	–	1.711	2.76	–	61	61
North Greenland	1.049	0.763	0.824	−27	8	−19
North and East Barents Sea	0.451	0.671	0.912	49	36	85
Northern Grand Banks - Southern Labrador	0.666	0.696	0.73	5	5	10
Northern Labrador	0.86	0.691	0.763	−20	10	−10
Northern Norway and Finnmark	0.751	1.056	1.129	41	7	48
Norwegian Sea	0.604	0.758	0.882	26	16	42
West Greenland Shelf	0.898	0.716	0.774	−20	8	−12
Western Bering Sea	0.508	0.829	0.861	63	4	67
White Sea	0.884	1.725	1.937	95	12	107
Total Artic Ocean	0.623	0.714	0.78	15	9	24

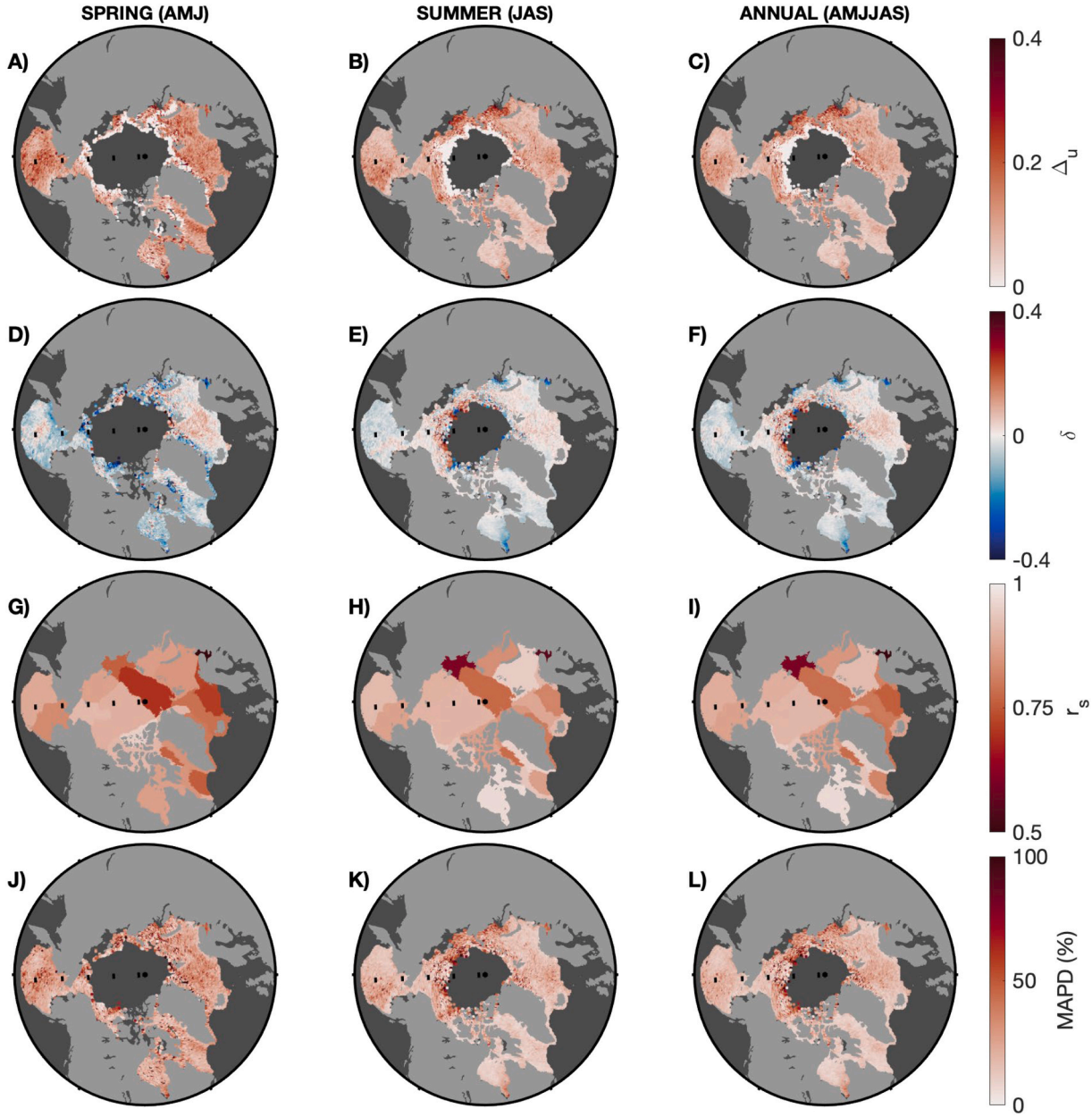

Fig. 5. SeaWiFS spatial statistical indices. Spatial distribution of the multi-annual seasonal averages of (A, B, C) unbiased RMS Δ_u, (D, E, F) bias δ, (G, H, I) bio-regional Spearman's correlation coefficient r_s and (J, K, L) Mean Absolute Percentage Difference (MAPD, %) obtained for the SeaWiFS sensor (1998–2006) comparing the NEW with the REF dataset. The black background corresponds to regions with no data because of sea-ice, masked areas (depth < 25 m) or outside the studied area. (For interpretation of the references to color in this figure legend, the reader is referred to the web version of this article).

were provided based on the ensemble of N pairs of valid Chl *a* from annual composites (AMJJAS) from all available years. The exhaustive multi-annual statistical results of this analysis are summarized using bar plots in Fig. 7**,** which also provides a qualitative ranking evaluating the relative performance in each bio-region for each log-transformed statistical index (see **Tables S10** to **S12** to see the actual quantitative ranking). Note that Δ_u, δ and r_s can also be visualized spatially in maps in the right panels of **Figs. 5** and **6** (for SeaWiFS and MODIS respectively).

4.1.2.1. Linear regressions (S, I, r_s). The Spearman's correlation coefficient for the White Sea was much smaller than the average (red line in Fig. 7A) for both SeaWiFS ($r_s = 0.47$, **Table S5**) and MODIS ($r_s = 0.61$, Fig. 7C**, Table S6**) compared to all other bio-regions, which exhibited correlation coefficients greater than 0.75 (p-values <0.001). The White Sea was discarded from further analyses and discussions. It is important to note that a few bio-regions were characterized by slopes that deviate by more than +/− 0.15 from the ideal 1:1 line slope such as the Atlantic basin of the AO ($S = 0.79$) and the southern Labrador ($S = 1.17$) for SeaWiFS (Fig. 7B). For MODIS, the southern Labrador Sea showed the largest deviation from the ideal slope ($S = 1.59$, Fig. 7G). The Hudson Complex and high Arctic Archipelago also showed noticeable deviations (S = 1.17 and 0.82). Results from these three bio-regions should therefore be interpreted with caution.

4.1.2.2. Unbiased Root Mean Square difference (URMS, Δ_u). Several Arctic bio-regions were characterized by differences in variability (Δ_u) that were higher than the average for the entire AO ($\Delta_{u\ \mathrm{SeaWiFS}} = 7.4\ 10^{-2}$ in Fig. 7D**, Table S5**; $\Delta_{u\ \mathrm{MODIS}} = 4.8\ 10^{-2}$ in Fig. 7I**, Table S6**). For example, the SeaWiFS NEW re-processing led to higher-than-average Δ_u in bio-regions from all sectors, including the Fram Strait ($\Delta_u = 9.8\ 10^{-2}$),

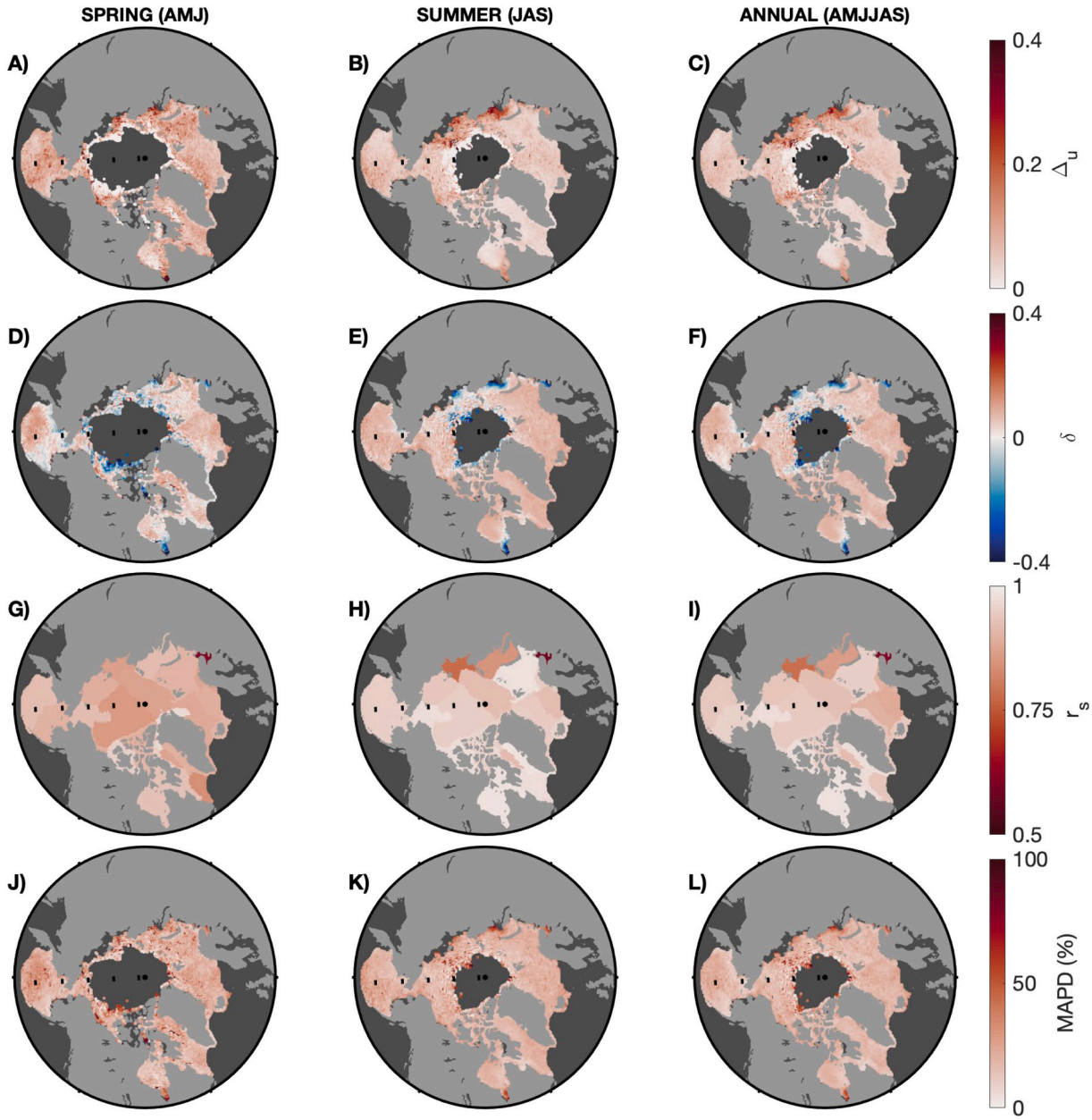

Fig. 6. MODIS spatial statistical indices. Spatial distribution of the multi-annual seasonal averages of (A, B, C) unbiased RMS Δ_u, (D, E, F) bias δ, (G, H, I) bio-regional Spearman's correlation coefficient r_s and (J, K, L) Mean Absolute Percentage Difference (MAPD, %) obtained for the MODIS sensor (2003–2016) comparing the NEW with the REF dataset. The black background corresponds to regions with no data because of sea-ice, masked areas (depth < 25 m) or outside the studied area. (For interpretation of the references to color in this figure legend, the reader is referred to the web version of this article).

the Beaufort continental shelf ($\Delta_u = 9.6\ 10^{-2}$) and the Kara Sea ($\Delta_u = 14.2\ 10^{-2}$). This general pattern remained similar for MODIS with the Russian shelves particularly affected by large Δ_u values.

4.1.2.3. Biases (δ). Biases (δ) also inform on discrepancies between NEW and REF. For SeaWiFS, several bio-regions (among which the Atlantic basin of the AO, the East and North Greenland shelves, the Hudson Complex and the southern Labrador Sea) had absolute biases that largely exceeded the pan-Arctic average ($\delta = -3\ 10^{-2}$, Fig. 7E). Similarly, for MODIS, few bio-regions (the Hudson complex, the Iceland shelf, the northern Norway and Finmark and the Norwegian Sea) were identified with bias substantially larger than the entire AO bias ($\delta = +5.6\ 10^{-2}$, Fig. 7J). The average bias between NEW and REF for SeaWiFS spring climatology at pan-Arctic scale was close to 0 on average. This resulted from both low bio-regional biases and the compensation between positive and negative biases in the Eurasian and Amerasian Arctic sectors, respectively.

4.2. Climatological inter-mission bias and comparison with in situ data

The bio-regional correction was an important step to remove the inter-mission bias between SeaWiFS and MODIS for the NEW dataset and to provide consistent time-series that account for spatial heterogeneities. The temporal overlap between SeaWiFS and MODIS missions allowed the comparison of Chl *a* during the months of April to September between 2003 and 2006. Prior to the correction of the bias, the AO average difference between the two datasets was already low, but not negligible, with an estimated MAPD value of 16.3%. The Chl *a* comparison between the two missions in terms of bias ($\delta_{MODIS\text{-}SeaWiFS}$) highlighted the higher Chl *a* levels derived using SeaWiFS than those

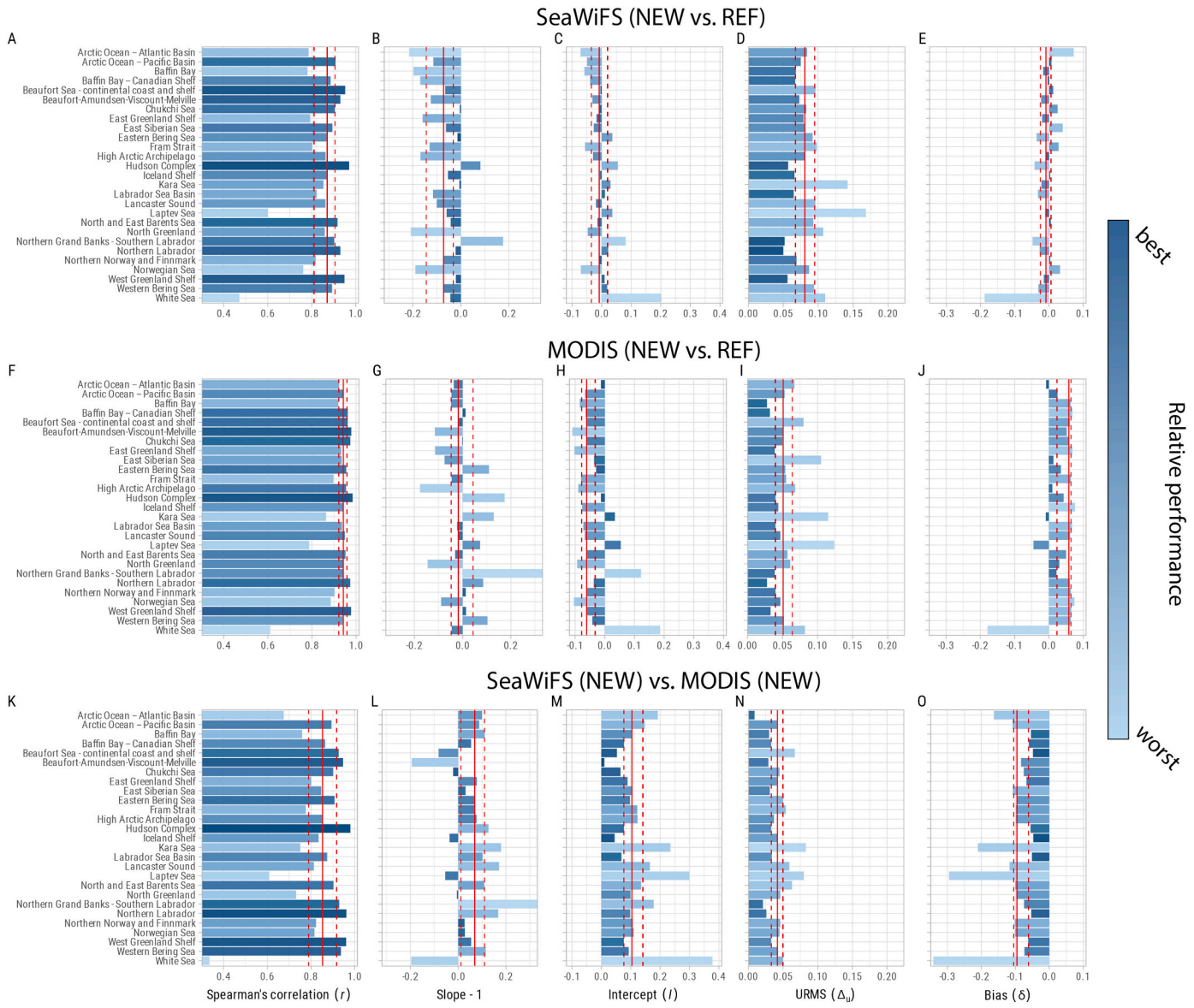

Fig. 7. Statistical indices. Illustration of the quality of annual composites of the re-processed dataset (NEW) compared to the reference product (REF) for SeaWiFS (1998–2006; top panels, A to E) and MODIS (2003–2016; middle panels, F to J), for all months. The re-processed SeaWiFS and MODIS datasets are also compared during their overlapping period (2003–2006; bottom panels, K to O). The blue palette is a qualitative indicator of the relative performance (i.e. ranking) of each statistical index in each of the 27 bio-regions: Spearman's coefficient correlation (r_s; A-F-K), Slope-1 (B-G-L), Intercept (I; C-H-M), unbiased RMS (Δ_u; D-I-N) and bias (δ; *E*-J-O). The red vertical solid line indicates the median over the 27 bio-regions while the red vertical dashed lines indicate the 25th and the 75th percentiles. (For interpretation of the references to color in this figure legend, the reader is referred to the web version of this article).

obtained using MODIS almost everywhere in the AO (negative bias in Fig. 7O and 8, see also **Tables S7–9**). Averaged over the AO, the bias was more important in spring ($\delta_{MODIS\text{-}SeaWiFS} = -9.3\ 10^{-2}$, Fig. 8D) than in summer ($\delta_{MODIS\text{-}SeaWiFS} = -5.6\ 10^{-2}$, Fig. 8E) with an annual average of $-7.2\ 10^{-2}$ (Fig. 8F). In spring, the spatial distribution of $\delta_{MODIS\text{-}SeaWiFS}$ was almost homogeneous throughout the AO. In summer, the largest $\delta_{MODIS\text{-}SeaWiFS}$ values were located on the Russian Arctic shelves whereas the $\delta_{MODIS\text{-}SeaWiFS}$ decreased everywhere else. All the MODIS climatologies (from daily to annual) were systematically corrected for the bias with the SeaWiFS dataset calculated on a pixel-by-pixel basis using the exact same time aggregation (e.g. spring climatologies were corrected with spring bias). The choice of correcting MODIS instead of SeaWiFS is further discussed in section 5. From now on, the NEW dataset refers to the dataset that includes the bias-corrected MODIS dataset.

The 2003–2006 climatologies of SeaWiFS and MODIS have also bio-regional differences in precision as expressed by Δ_u which cannot be corrected from one mission to another. However, the annual average Δ_u over all bio-regions remained reasonably low ($\Delta_u = 3.4\ 10^{-2}$, red vertical line in Fig. 7N). Seven bio-regions in total had distinctly higher Δ_u than average (Fig. 7N, **Table S9**). Among others, this list includes the Beaufort continental shelf ($\Delta_u = 6.7\ 10^{-2}$) and the Laptev Sea ($\Delta_u = 8\ 10^{-2}$).

Validation of satellite-derived properties is challenging due to the different spatial scales between satellite and in situ measurements and of the lack of matchups in the AO to provide results with statistical meaning. The difficulty is amplified when assessing the performance of CZCS observations as they were collected about 40 years ago, when in situ Chl *a* pigments were generally measured using fluorescence-based or spectrophotometric methods without standardized procedures. Nevertheless, Chl *a* from the NEW dataset were compared with an in situ database made of all in situ Chl *a* found north of 45°N in the World Ocean (https://www.ncei.noaa.gov/access/world-ocean-database-sele

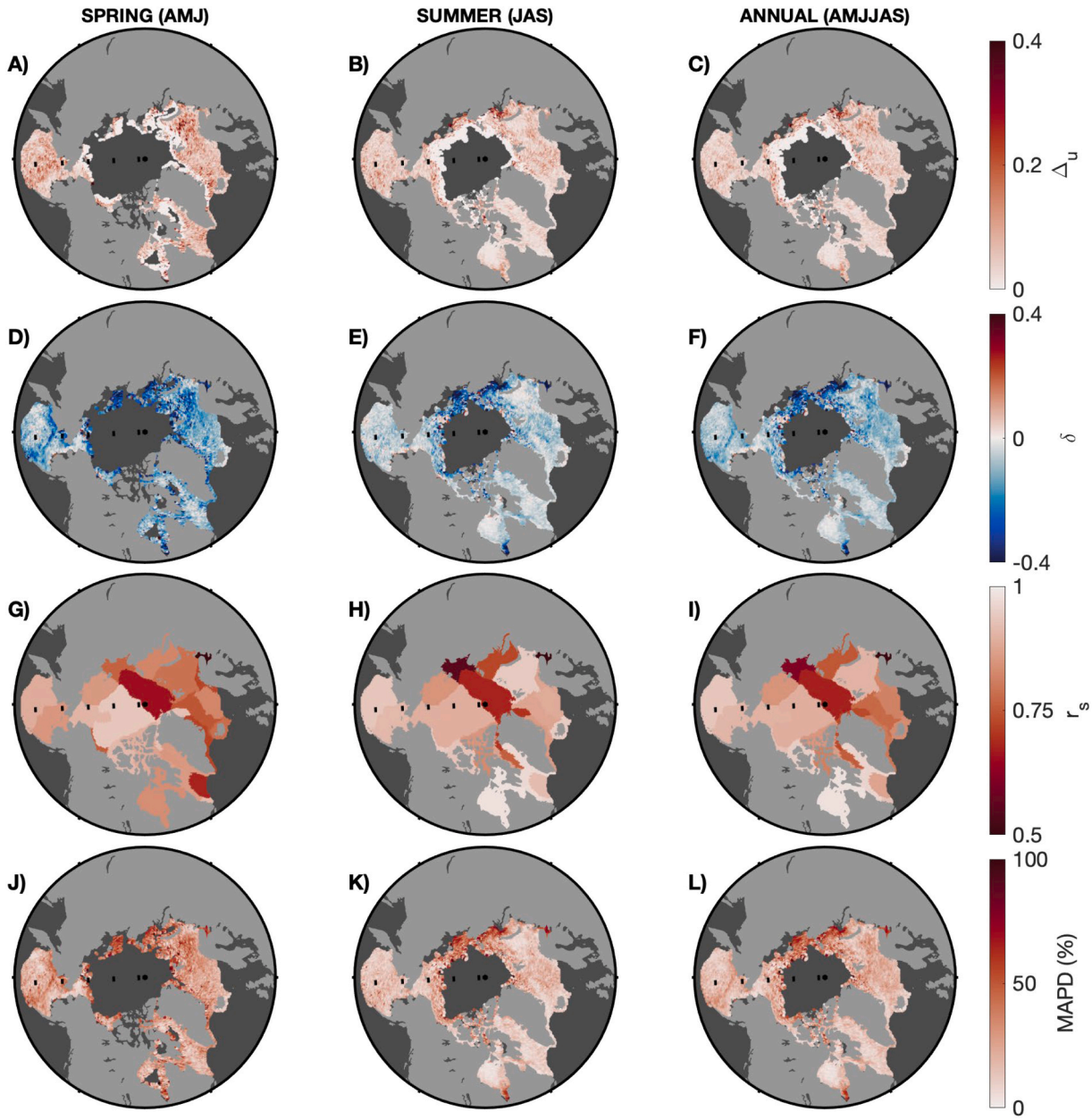

Fig. 8. Spatial statistical indices comparing SeaWiFS and MODIS. Spatial distribution of the multi-annual seasonal averages of (A, B, C) unbiased RMS Δ_u, (D, E, F) bias δ (MODIS – SeaWiFS), (G, H, I) bio-regionnal Spearman's correlation coefficient r_s and (J, K, L) Mean Absolute Percentage Difference (MAPD, %) obtained comparing SeaWiFS and MODIS (2003–2006). SeaWiFS tends to over-estimate Chl *a* compared with MODIS especially in spring. The black background corresponds to regions with no data because of sea-ice, masked areas (depth < 25 m) or outside the studied area. (For interpretation of the references to color in this figure legend, the reader is referred to the web version of this article).

ct/dbsearch.html) and ICES (https://ocean.ices.dk/) databases. We excluded the European North and Baltic Seas which produced almost exclusively outliers likely due to their specific optical signature resulting from terrigenous inputs. In addition, results from the matchup analysis are affected by the quality of the fluorescence-estimated Chl *a*, which could not be warranted, and the reduced spatial resolution of the pixels used in the matchups (~28-km resolution), which was selected to increase the number of matchups for CZCS (from less than 10 with the 4-km resolution to 147 with the 28-km resolution). The match-up exercise shown in Fig. 9, was carried out using 147, 3202 and 3775 available in situ and satellite Chl *a* pairs for CZCS, SeaWiFS and MODIS sensors, respectively. CZCS showed a significant Pearson's correlation r of 0.54 (type II regression, *p*-value $<10^{-4}$) with a slope of 0.72, similar to the slopes found for SeaWiFS (S = 0.76) but smaller than the one found for MODIS (S = 0.90). Both SeaWiFS and MODIS datasets showed similar correlation coefficients of about 0.2. The intercept for CZCS (−0.15) was greater than the one found for SeaWiFS and MODIS, which were close to zero (0.047 and 0.074 respectively).

4.3. Climatologies and decadal changes

Seasonal (spring and summer) Chl *a* climatologies derived from the NEW dataset (CZCS, 1979–1984; SeaWiFS, 1998–2006; and MODIS, 2007–2016, corrected from bias) illustrate the spatial distribution of Chl *a* distribution and the shrinking sea-ice extent (seasonal climatology of minimum sea-ice concentrations >10%) recorded during the successive satellite missions (Fig. 10 and Table. 1). Indeed, the use of climatologies ensures 100% data coverage and missing pixels are only due to the

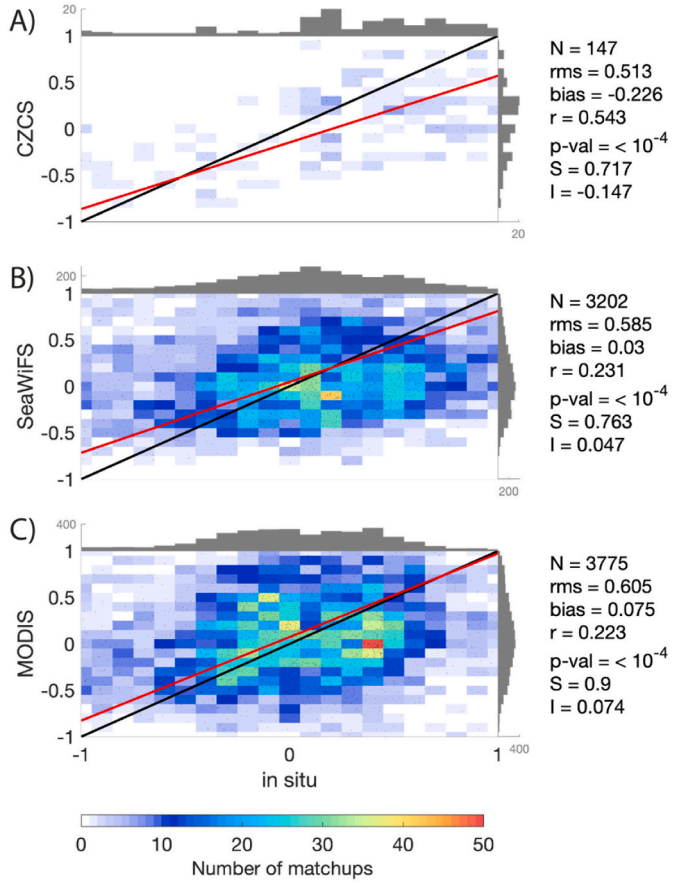

Fig. 9. Comparison of remotely sensed (y-axis) versus in situ observations (x-axis) of Chl *a* concentration. Results are shown in $\log_{10}$(Chl *a*) [mg m^{-3}] scales on both x and y-axis. To ensure readability, data points were superimposed on the density-plots indicating the number of match-ups within each regular bin (with a 0.1 resolution). The x and y distributions are also illustrated by histograms on the top and right hands, showing the number of match-ups per bins. The black line indicates the 1:1 line while the red solid line represents the linear regressions. Statistics of the type II regression are shown on the right-hand side: number of match-ups (N), root mean square difference (RMS), Pearson's correlation coefficient (r), slope (S) and intercept (I). Note that match-ups were calculated from daily maps with a 28-km resolution. (For interpretation of the references to color in this figure legend, the reader is referred to the web version of this article.)

presence of sea-ice (besides masked areas such as non-Arctic regions and depths shallower than 25 m). The Russian shelves were almost entirely ice covered during the CZCS era. The Chl *a* climatologies show similar spatial distributions for the three sensors with (i) the highest Chl *a* values observed in the inflow shelves (Barents and Bering Seas) in spring while the high AO is still covered with sea-ice, (ii) the highest Chl *a* values observed in summer in the Seasonal Ice Zone such as in the interior shelves (sensu Carmack and Wassmann 2006; e.g. Russian shelves), and (iii) the lowest Chl *a* found in the central Arctic and in the outflow shelves (e.g. Baffin Bay, Greenland Seas). However, the magnitudes suggest a chronological increase in Chl *a* from the CZCS to the SeaWiFS period, and from the SeaWiFS to the MODIS period.

Those decadal changes were better illustrated by computing the pixel-by-pixel (Fig. 11) and bio-regional (Table. 1) differences in Chl *a* levels between missions. A strong increase occurred in most Arctic regions in Spring from the 1979–1984 climatology to the 1998–2006 one (Fig. 11A), especially in the western Bering Sea, the Norwegian Sea and the Barents Sea with local values greater than +0.6 $\log_{10}$(Chl *a*) [mg m^{-3}]. A decrease in Chl *a* can be observed in the vicinity of the American continent such as in the eastern Bering Sea, and some western parts of the Labrador basin and Fram Strait. This trend was generally continued from the 1998–2006 to the 2007–2016 periods (Fig. 11B) where almost all of the AO showed positive changes in Chl *a,* except in the eastern Bering Sea which still experienced negative changes. In summer, the increase in Chl *a* from the CZCS to the SeaWiFS era were limited to the sub-Arctic Seas (Icelandic Sea, Labrador basin, Bering Seas, northern Norway) and inflow shelves (Barents Sea, Chukchi Sea, Fig. 11C). Smaller changes occurred everywhere else, mostly around Greenland and America. These same regions (i.e. Greenland and Canada area) experienced changes in the evolution of the Chl *a* from the SeaWiFS to the MODIS periods Fig. 11D) while the increase in the inflow shelves (Chukchi and Barents Seas) continued. The difference between MODIS and SeaWiFS in summer revealed a strong positive increase in the Russian Seas, where almost no data were available during the CZCS era. When averaged both annually (Fig. 11E, F) and bio-regionally, (Table 1), results confirmed the change of sign (from negative to positive values) in the evolution of Chl *a* in most Canadian Arctic areas (e.g. Baffin Bay: −24% to +29%) and the East Greenland Shelf (−27% to +19% on the eastern shelf). The opposite scenario occurs in the eastern Bering Sea where the increase from the 80s to the early 2000s (+18%) was followed by a decrease in the 2010s (−15%). By contrast, the Barents Sea was consistently characterized by Chl *a* increase over several decades of observations (+49% and + 36%). At pan-Arctic scale (the whole studied area), results showed a total increase of +24% in Chl *a*, with +15% from CZCS to SeaWiFS and + 9% from SeaWiFS to MODIS.

5. Discussion

The main outcome of the quality assessment of the NEW dataset, when compared to REF, is that the 'CZCS-like' re-processing of SeaWiFS and MODIS had limited impact on Chl *a* distribution over the AO. The differences (MAPD) averaged over the AO were about 20% and provides a good level of confidence. In comparison, satellite-derived Chl *a* in the Global Ocean usually show differences of ±35% relative to the reference value (Bailey and Werdell, 2006; Hooker and Esaias, 1993; McClain et al., 2006). The MAPD derived for the overlapping period between SeaWiFS and MODIS were about 16% (before correction) which corresponds to the lower bound of the usual range in Chl *a* difference found between SeaWiFS and MODIS in other studies (20–35%, e.g. Melin, 2010).

The statistical indices computed to compare NEW and REF for all the 27 bio-regions (Fig. 7**)** showed, in general, high Spearman's correlation coefficients ($r_s > 0.8$), low unbiased RMS differences (<0.1) and biases (< 0.01). Those results confirmed a good agreement between the REF and the NEW datasets similar or even better performances than inter-sensors comparison in the global Ocean (e.g. Djavidnia et al., 2010). In that sense, the NEW SeaWiFS and MODIS datasets do not seem particularly altered by the use of CZCS atmospheric correction and the application of the Morel-3 algorithm to derive Chl *a*. In future studies, it would also be interesting to compare the NEW dataset with the recently improved GSM-based algorithm (AO.GSM, Lewis and Arrigo, 2020). The NEW dataset presents the unique advantage of expanding the temporal coverage of ocean color in the Arctic Ocean to the late 70's and early 80's. The quality of the decadal change assessment relies on several factors such as the quality of the inter-mission bias correction, and more importantly, data availability. In the following section, we address the quality of the NEW Chl *a* dataset, and we discuss the implications for the observed Chl *a* changes.

5.1. Re-processing of SeaWiFS and MODIS: which bio-region gives the most reliable Chl a estimates?

The bio-regional approach to quantify uncertainties in satellite-derived Chl *a* demonstrated that all oceanic Arctic regions exhibit singular remotely sensed optical properties that affect satellite-based Chl *a* estimations differently in time and space. The purpose of the bio-

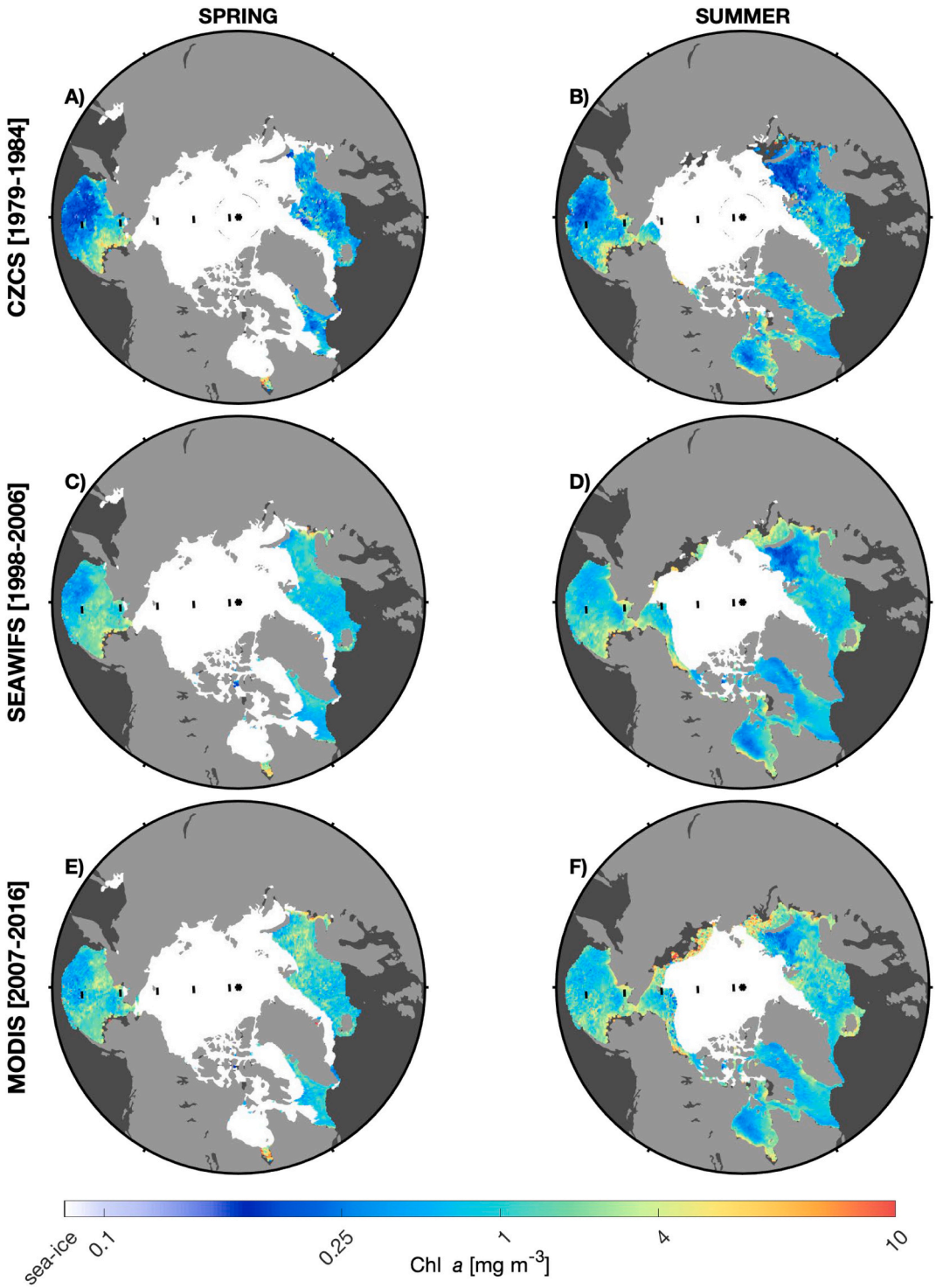

Fig. 10. Seasonal climatological maps of log_{10}-transformed Chl *a* [mg m^{-3}]. Spring (left) and summer (right) Chl *a* maps for (A, B) CZCS (1979–1984), (C, D) SeaWIFS (1998–2006) and (E, F) MODIS (2007–2016, corrected from bias) with associated minimum sea-ice extent in white color (mean sea-ice concentration > 10% over the climatological period). The black background corresponds to regions with no data because of sea-ice, masked areas (depth < 25 m) or outside the studied area. (For interpretation of the references to color in this figure legend, the reader is referred to the web version of this article).

regional approach was to summarize large-scale Chl *a* changes into bio-region in which we assumed consistent and similar bio-optical properties. Note however that heterogeneous bio-optical regimes can occur at the intra-regional scales. For example, James Bay located in the south-western part of the Hudson Complex has been identified as an area with large variations in optical properties and is not always representative of the Hudson Complex (Granskog et al., 2007). It is important to keep in mind that most bio-regions are closely related with specific topographic features, but some bio-regions encompass both coastal and open waters for which one can expect different optical regimes. The coastal environments are subject to terrigenous inputs, particle resuspension, while open water bio-optical properties are driven mainly by phytoplankton. In this study, we used a Chl *a* algorithm adapted to the AO oceanic conditions. Hence, its application in coastal areas can lead to large

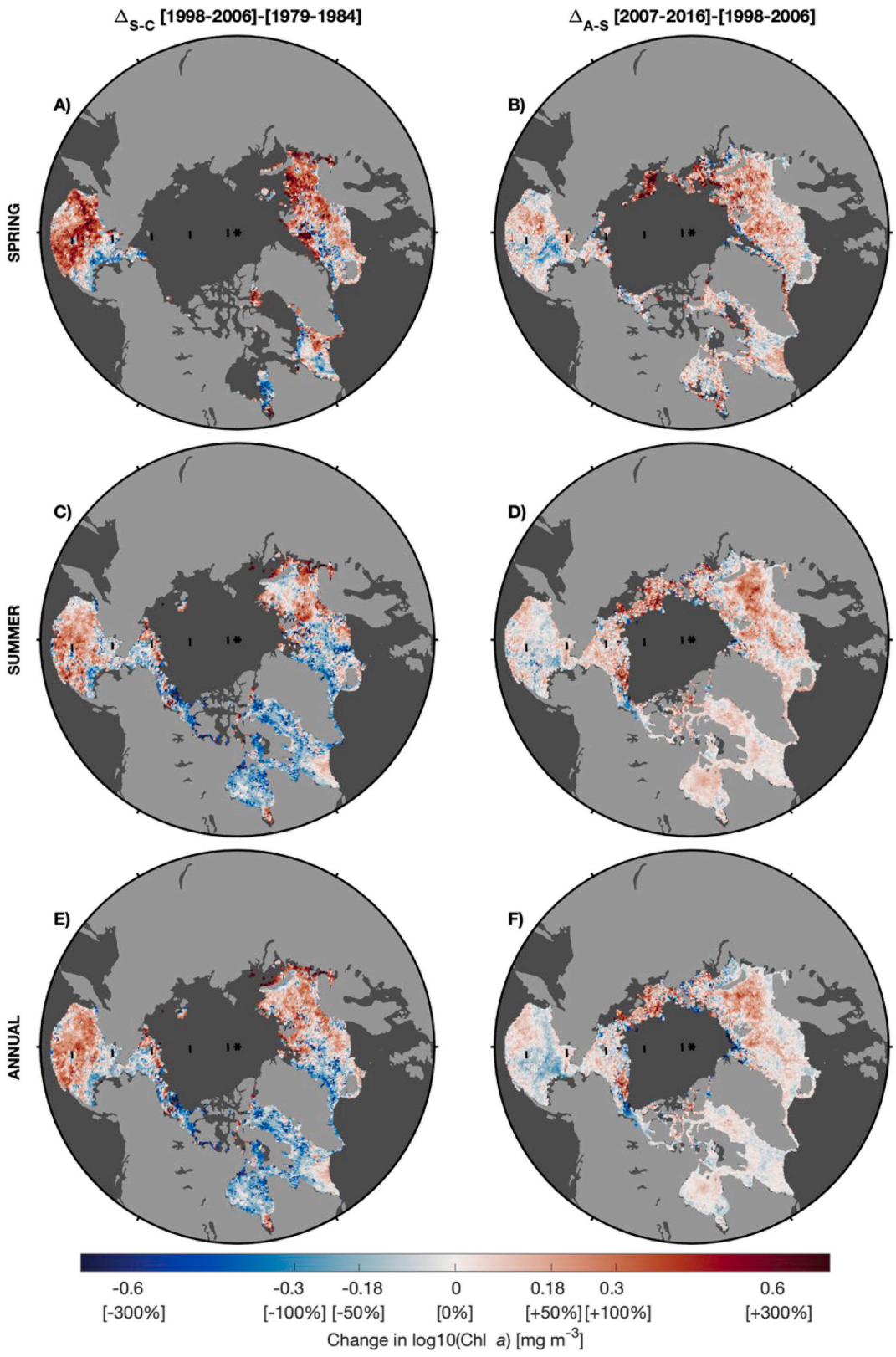

Fig. 11. Maps showing changes in Chl *a* in $\log_{10}$(Chl *a*) [mg m^{-3}] scale during (A, B) spring, (C,D) summer and (E, F) annual periods. Relative changes in linear scale are also shown in percentage [%]. On the left hand, maps show pixel-by-pixel differences between the SeaWiFS [S] and the CZCS [C] periods ([2006–1998] – [1979–1984]). On the right hand, maps show the differences between the MODIS [A] and the SeaWiFS climatologies ([2007–2016] – [1998–2006]). The difference between the two periods illustrates the increase (red) or decrease (blue) in Chl *a*. The black background corresponds to regions with no data because of sea-ice, masked areas (depth < 25 m) or outside the studied area. (For interpretation of the references to color in this figure legend, the reader is referred to the web version of this article.)

uncertainties. Results from several bio-regions have to be interpreted with caution at both the seasonal and annual scale (see next section). Bio-regions with little amount of data and/or with terrestrial inputs showed lower correlation coefficient between the NEW and REF datasets ($r_s < 0.75$, Fig. 7). These bio-regions did not meet an acceptable level of confidence to be included in the analysis. Therefore, we chose not to interpret results from flagged regions such as the White Sea, the central Arctic in spring or the Laptev Sea in summer.

The bio-regional division used in this study (Spalding et al., 2012) is currently one of the most detailed for the AO. However, in a context of rapid climatic changes in the AO and poleward shifts linked to the so-called 'borealization' of the Arctic ecosystems (e.g. Fossheim et al., 2015), it seems reasonable to assume that the bio-regions actually evolved over the study period. It is thus important to contextualize the results from one bio-region together with its adjacent ones before drawing any conclusion.

5.2. The inter-mission bias and in situ comparison

i) CZCS. Given the absence of overlap with other ocean color sensor, one way of assessing the possible bias of CZCS Chl *a* was to perform a comparison with in situ data. This was particularly challenging given the lack of reliable in situ data collected in the early 1980s. Nowadays, the space agencies recommend the use of HPLC-based Chl *a* estimations for validation of satellite-based measurements, while our study relied on fluorescence-based estimations. The combination of the lack of quality assessment of in situ data, the limited number of match-ups for CZCS ($N = 147$, Fig. 9A) and the coarse resolution of satellite data (~28 km maps used to ensure a sufficient number of match-ups to reach statistical significance) are complicating the assessment of CZCS Chl *a*. However, the results of the comparison between ocean color estimations and in situ observations were within the range found in the literature for current sensors (Fig. 9). The (type II) regression of satellite-derived against in situ Chl *a* showed a significant correlation ($r^2 = 0.54$, *p-value* < 0.01) with a slope of 0.72, an intercept of −0.15 and an unbiased RMS of about 0.5. For comparison, Lewis and Arrigo (2020) tested on SeaWiFS and MODIS their new 'state-of-the-art' Arctic-adapted semi-analytical algorithm and found results similar $r^2 \sim 0.58$ and RMS ~ 0.46.

Furthermore, in order to compensate for the low number of match-ups for CZCS ($N = 147$), a bootstrap evaluation was performed by repeating 1000 times the regression (model II) with a random sub-sampling (75%) of the initial matchups dataset. The bootstrap evaluation provided the 95% confidence intervals of the parameters derived from the comparison between CZCS and in situ data presented on Fig. 9A. Distributions for the bootstrap-estimated intercepts, slopes, unbiased RMS and Pearson's correlation coefficients are presented in **Fig. S5**. Lower and upper 95% intervals for the slope and intercept were respectively of 0.63–0.83 and − 0.22 – −0.08 with averages of 0.72 and − 0.15 respectively (identified using vertical dashed lines in **Fig. S5**). The average unbiased RMS and correlation coefficient were 0.33 and 0.54 respectively. The statistics found with the bootstrap evaluation are very similar than the regression derived with all match-ups in Fig. 9A with relatively narrow confidence intervals which confirms the robustness of the regression despite the low number of match-ups.

Overall, CZCS showed, like previous examinations (Evans and Gordon, 1994), reasonably good performances at predicting Chl *a*, at least similar to modern sensors and algorithms. Those results suggest that no further bias correction would improve the performance of Chl *a* retrievals. In fact, an additional bias correction may add uncertainties to the Chl *a* estimations due to the poor spatio-temporal coverage and the intrinsic uncertainties of the in situ data (i.e., fluorometric method without a standardized protocol).

Since no inter-mission bias correction was applied to CZCS, one may question the possible effect of SeaWiFS-CZCS uncorrected bias on the quantification of Chl *a* changes between the two sensors. One way to address this issue is to compare the differences observed between CZCS and SeaWiFS and the inter-mission bias between SeaWiFS and MODIS, both in terms of distribution and magnitude (**Fig. S6**). Results showed that SeaWiFS generally produced higher values of Chl *a* than the ones produced by MODIS during their overlapping period. Another study showed that MERIS and MODIS/Terra derived Chl *a* exhibited both positive and negative biases at the global scale (Djavidnia et al., 2010). In both cases (from this study and from the literature), inter-mission biases seem to be quasi-homogenous at basin scale. By contrast, the differences observed between CZCS and SeaWiFS were more heterogeneously distributed across the basins than the SeaWiFS-MODIS inter-mission bias (**Fig. S6**). This suggests that the observed differences in Chl *a* are less influenced by a systematic inter-mission bias than by a true change in phytoplankton biomass. In the presence of a systematic inter-mission bias between CZCS and SeaWiFS, the differences would be more evenly distributed spatially across the bio-regions, which was not evidenced (**Fig. S6**). In terms of magnitude, however, the MODIS-SeaWiFS inter-mission bias can be of similar or even greater magnitude than the changes in Chl *a* between the CZCS and SeaWiFS periods. This leads us to use caution in interpreting the results, as a possible uncorrected bias between SeaWiFS and CZCS may affect the magnitude or the sign of the Chl *a* changes (**Fig. S7**).

ii) SeaWiFS and MODIS. The bias correction consisted of removing the climatological bias between the NEW SeaWiFS and MODIS datasets during their overlapping period (2003–2006). As a consequence, the percentage Chl *a* difference between the two datasets was divided by a factor of two (MAPD decreased from ~16% to ~8% between 2003 and 2006, Fig. 8). In general, MODIS-derived Chl *a* estimations were slightly lower than those estimated from SeaWiFS. The inter-mission bias correction was also affected by the seasonal cycle of Chl *a* and was generally greater in the sub-Arctic regions due to generally larger Chl *a* values than in the high AO, especially in spring. The seasonal and bio-regional approaches provided a mean to locally correct the bias by accounting for the bio-optical heterogeneity of the AO. The Chl *a* RMS differences between REF and NEW (Δ_u) from SeaWiFS were generally greater than those from MODIS. This result suggests that MODIS Chl *a* estimations are more precise than SeaWiFS estimations. Unfortunately, the remaining RMS difference (Δ_u) between NEW SeaWiFS and MODIS cannot be corrected by a simple bias correction as it corresponds to a non-systematic dispersion of the data. Validation with in situ data was performed after correction of MODIS inter-mission bias. The choice of correcting MODIS instead of SeaWiFS was motivated by the fact that the re-processed SeaWiFS NEW dataset had smaller biases than the MODIS NEW one (compared with REF, see Fig. 7, 8D-E-F) and in line with previous multi-mission studies (Gregg and Rousseaux, 2014; Mélin et al., 2016). This choice was also supported by the comparison against in situ data as the correction of MODIS bias improved the matchups statistics by increasing the slope of the linear regression from 0.78 to 0.9 while the intercept remained unchanged. On the contrary, correcting SeaWiFS would have degraded the results by lowering the slope from 0.76 to about 0.64 (results not shown).

5.3. Data coverage and the presence of sea-ice: a non-negligible limitation of ocean color remote sensing observations

Data coverage is generally the most important limiting factor for reliable calculation of Chl *a* climatologies and quantification of changes. The construction of 28-km resolution monthly composite maps artificially decreased the influence of clouds. When aggregated into seasonal or annual climatologies, the absence of data was systematically attributed to the presence of sea-ice. Because sea ice extent decreased significantly during the last four decades, ocean color remote sensing data spatial coverage increased with time (Fig. 3). As a result, the 1998–2016 (SeaWiFS-MODIS) period was characterized by more ice-free (and therefore documented) bio-regions than during the 1979–1984 (CZCS) period. During spring, only the Atlantic and Pacific sub-Arctic sectors (year-round or seasonally ice-free) contained enough

data for analysis in the early 80s. In comparison, open waters, and therefore information on Chl *a* occurred at least in three additional bio-regions located in the Labrador Sea and Baffin Bay. In summer, the increase in data coverage in recent years is even more obvious as new observations are appearing for all the Russian shelves, the Canadian sectors and the central AO (Pacific and Arctic basins).

5.4. Decadal changes in Chl a

The addition of the CZCS time series to the modern ocean color remote sensing era provides a valuable phytoplankton biomass baseline in the AO, and helps quantifying and understanding the changes that occurred before the triggering of the linear sea-ice loss during the late 1980s in the AO (Peng and Meier, 2018). This glimpse into the recent past highlights interesting features in the Chl *a* decadal changes for the AO that are documented for the first time (Fig. 10):

(1) The first major outcome is that the exhaustive quality assessment of the dataset provided sufficient warranties to ensure reliable multi-annual variability analysis in most of the AO where data coverage was appropriate.
(2) Chl *a* increased of about +24% over the AO since 1979. Our study therefore highlights that the increase previously documented from 1998 to current time actually started four decades ago and occurred throughout both in spring and summer.
(3) In the AO, the bio-regions located in the inflow shelves accounted for most of the increase in Chl *a* since 1979. The top five bio-regions with continuous Chl *a* increase are: 1) the Barents Sea [+85%], the western Bering Sea [+67%], the northern Norway and Finnmark [+48%], the Norwegian Sea [+42%] and the Chukchi Sea [+16%].
(4) The interior shelves (Kara, Laptev and Siberian Seas) were almost completely covered by sea-ice throughout the spring and summer during the CZCS era. Therefore, we could only rely on a few measurements to quantify Chl *a* changes between the CZCS and SeaWiFS periods but one could consider that the appearance of these newly opened waters represented an addition in Chl *a* for the AO. The Chl *a* changes in the interior shelves were the largest recorded with +151%, 88% and + 61% for the Kara, East Siberian and Laptev Seas respectively.
(5) Another major outcome of our study concerns the area in the vicinity of the Canadian archipelago and Greenland. In this particular area, Chl *a* decreased from CZCS to SeaWiFS and then increased from SeaWiFS to MODIS. This was particularly true for the Baffin Bay, the Labrador Sea and the Greenland shelves. This scenario would suggest a decrease from 1979 to an inflexion point that occurred during the data gap (1986–1998).

Comparing those results with previous work is challenging given the methodological differences used in other ocean color remote sensing studies and the small number of time series from both in situ observation and modeling studies. However, the Chl *a* increase of 24% observed here for the whole AO remains in the same order of magnitude than observed in other ocean color remote sensing studies. For example, Lewis et al. (2020) found a trend of +21.6% for the 1998–2018 period. Previous studies attributed the increase in phytoplankton productivity in the AO to an increase in light availability due to the loss of sea-ice resulting in larger open water areas and longer growth seasons (Arrigo et al. 2008; Arrigo and van Dijken, 2015; Bélanger et al., 2013). However, Bélanger et al. (2013) insisted that most of the net primary production increase during the SeaWiFS period (1998–2010) was primarily due to increase in Chl *a*. A recent study (Lewis et al., 2020) suggested an increasing role for nutrient fluxes in the acceleration of the Chl *a* increase in recent years.

At the regional scale, previous ocean color remote sensing studies also evidenced that the largest Chl *a* increase occurred in the inflow shelves such as the Barents and Chukchi Seas during the SeaWiFS and MODIS periods (Lewis et al., 2020) while outflow shelves were characterized by much weaker trends (i.e. in the vicinity of Canada and Greenland; Bélanger et al., 2013; Lewis et al., 2020). Our results are consistent with the concept that the inflow shelves are 'hotspots' where phytoplankton biomass increases the most. The extension of the time series to the 1980s could lead to review upward previous estimations of primary production increase over the AO. The decrease in Chl *a* in the outflow shelves between CZCS and SeaWiFS periods is a surprising new result that might be explained by local processes. For example, Blais et al. (2017) combined remote sensing and in situ measurements to show a significant decrease in the northern Baffin Bay phytoplankton biomass between 1998 and 2011 in fall. The authors demonstrated that those changes were linked to sea-ice and freshwater dynamics which intensified stratification, confirming results obtained earlier by Tremblay et al. (2012). Unfortunately, only a few other studies have gathered in situ samples before the late 1990s. Hill et al. (2018) attempted to derive trends in the Pacific Arctic based on in situ primary production measurement but concluded that the objective was unreachable given the lack of field observations. Another interesting attempt at deriving multi-annual Chl a trends from observation was conducted by Nöthig et al. (2020) but was limited to the Fram Strait only and started in 1991. The authors did not find any significant trend. Similarly, only a few modeling studies can provide long enough historical time series that starts before the 1990s (e.g. Kinney et al., 2020). Future modeling projections predicted a continued (1) decrease in phytoplankton productivity in the outflow shelves until the end of the century mainly because of ice-melt induced increased stratification (Slagstad et al., 2015); (2) increase in primary productivity in the inflow and interior shelves at least until 2050 when the system would eventually become limited in nutrient (Slagstad et al., 2015; Vancoppenolle et al., 2013), although the latter conception of the future Arctic Ocean is now challenged by studies showing a possible increase in the annual budget of nutrient (i.e. Ardyna et al. 2014, Lewis et al., 2020).

6. Conclusion

This study created the longest, compatible with global change studies, inter-sensor calibrated Chl *a* time series (37-years, 1979–1984 and 1998–2016) in the Arctic Ocean by connecting data from the first ocean color CZCS sensor with SeaWiFS and MODIS sensors (1998–2016). This was achieved by: (1) re-processing the entire SeaWiFS and MODIS time series with a similar atmospheric correction scheme than CZCS and applying the same Chl *a* algorithm (i.e., two-band ratio) to the three sensors in order to ensure homogeneity and consistency of the data for global change study; (2) correcting SeaWiFS-MODIS inter-mission biases; and (3) assessing the quality of the re-processed dataset by comparison with recent remotely sensed time series as well as in situ data. The quality assessment demonstrated that the re-processing did not alter the quality of the dataset which is particularly well adapted for large scales and decadal studies. However, regional statistical analysis showed a spatial heterogeneity in the quality of the satellite-derived Chl *a*. A bio-regional approach provided a mean to exclude areas with unreliable data due to large discrepancies with a reference dataset. An important limitation of the CZCS dataset lies in its poor data coverage, which was addressed by a careful spatio-temporal aggregation. Despite those identifiable discrepancies, the addition of CZCS data to current time series offers several unique benefits including: the definition of baseline conditions in phytoplankton biomass in the Arctic Ocean for the early 1980s before the acceleration of sea-ice melt, a better characterization of decadal changes due to the longer period of observation (almost doubled), and further insight into the regional response of phytoplankton biomass to a changing Arctic Ocean. Our study confirmed for example that the mean Chl *a* increase in the AO by about +24% between 1979 and 2016. The strongest increase in the mean Chl *a* occurred in the Russian shelves which were heavily ice

covered during the CZCS era. The Kara, Laptev and Siberian Seas experienced a total increase of +151%, 107% and 88% respectively. The rest of the increase was attributed to the inflow shelves: the Barents Sea and the western Bering Sea. The two regions continuously showed among the strongest increase since 1979 with +85% and 67% respectively. Perhaps, and more interestingly, the Chl *a* levels were higher in the 1980s in the outflow shelves such as in the Baffin Bay area than in present time suggesting either a decreasing trend or a decadal oscillation.

Author contributions

L.O., M.B., and E.D. conceptualized this study. L.O produced the dataset with help from E.D. L.O. conducted the data analysis with help from E.D. and P.M. L.O. wrote the manuscript. All authors (L.O., P.M., M.B. and E.D.) contributed to the ideas and edited the manuscript.

Additional information

Supplementary information is available for this paper at.

Data availability

All the raw data used in this research are freely available to the public and may be downloaded through the links detailed in the Methods section. The quality-controlled databases (i.e. NEW dataset, seasonal and annual Chl *a* climatological composite maps, corrected from inter-mission biases) are publicly available from the SEANOE (SEA scieNtific Open data Edition) publisher at doi:10.17882/86601 (Oziel et al., 2022). The REF dataset is not publicly available and is processed and stored in Takuvik laboratory, and can be made available on request.

Declaration of Competing Interest

The authors declare no competing interests.

Acknowledgements

L.O. was funded by an NSERC/CRSNG “Visiting Fellowship” in Canadian laboratories in the framework of the DFO-International Governance Strategy (IGS project, PI: Emmanuel Devred). L.O. was also supported by the joint international laboratory Takuvik (ULaval/CNRS), the Canada Excellence Research Chair in remote sensing of Canada’s new Arctic frontier. This study was also a contribution to the Green Edge project which is funded by the following French and Canadian programs and agencies: ANR (Contract #111112), CNES (project #131425), IPEV (project #1164), CSA, Fondation Total, ArcticNet, LEFE and the French Arctic Initiative (Green Edge project). The authors would like to warmly thank Sean Bailey and NASA OPGB Group for assistance in the gathering of MODIS L1A files, Maxime Benoit-Gagné for the calculation of the Chl *a* with the GSM01 algorithm and Martí Galí Tàpias for the binning algorithm. Note that this study heavily relied on massive computer calculations and would not have been possible without the decisive implication and assistance of Compute Canada (www.computecanada.ca) and Calcul Quebec. Note that the dataset is currently being updated from 2016 to present time.

Appendix A. Supplementary data

Supplementary data to this article can be found online at https://doi.org/10.1016/j.rse.2022.113020.

References

Ahmad, Z., Franz, B.A., McClain, C.R., Kwiatkowska, E.J., Werdell, J., Shettle, E.P., Holben, B.N., 2010. New aerosol models for the retrieval of aerosol optical thickness and normalized water-leaving radiances from the SeaWiFS and MODIS sensors over coastal regions and open oceans. Appl. Opt. 49, 5545–5560. https://doi.org/10.1364/AO.49.005545.

Antoine, D., Morel, A., Gordon, H.R., Banzon, V.F., Evans, R.H., 2005. Bridging ocean color observations of the 1980s and 2000s in search of long-term trends. J. Geophys. Res. Ocean. 110, 1–22. https://doi.org/10.1029/2004JC002620.

Ardyna, M., Babin, M., Gosselin, M., Devred, E., Rainville, L., Tremblay, J.E., 2014. Recent Arctic Ocean sea ice loss triggers novel fall phytoplankton blooms. Geophys. Res. Let. 41, 6207–6212. https://doi.org/10.1002/2014GL061047.

Arrigo, K.R., van Dijken, G., Pabi, S., 2008. Impact of a shrinking Arctic ice cover on marine primary production. Geophys. Res. Let. 35, 1–6. https://doi.org/10.1029/2008GL035028.

Arrigo, K.R., van Dijken, G.L., 2015. Continued increases in Arctic Ocean primary production. Prog. Oceanogr. 136, 60–70. https://doi.org/10.1016/j.pocean.2015.05.002.

Babin, M., Arrigo, K., Bélanger, S., Forget, M.-H., Frouin, R., Hill, V., Hirawake, T., Matsuoka, A., Mitchell, B.G., Reynolds, R.A., 2015. Ocean Colour Remote Sensing in Polar Seas, IOCCG, Repo. ed. IOCCG, International Ocean Colour Coordinating Group, Dartmouth, Canada.

Bailey, S.W., Werdell, P.J., 2006. A multi-sensor approach for the on-orbit validation of ocean color satellite data products. Remote Sens. Environ. 102, 12–23. https://doi.org/10.1016/j.rse.2006.01.015.

Beaulieu, C., Henson, S.A., Sarmiento, J.L., Dunne, J.P., Doney, S.C., Rykaczewski, R.R., Bopp, L., 2013. Factors challenging our ability to detect long-term trends in ocean chlorophyll. Biogeosciences 10, 2711–2724. https://doi.org/10.5194/bg-10-2711-2013.

Bélanger, S., Babin, M., Tremblay, J.-É., 2013. Increasing cloudiness in Arctic damps the increase in phytoplankton primary production due to sea ice receding. Biogeosciences 10, 4087–4101. https://doi.org/10.5194/bg-10-4087-2013.

Ben Mustapha, Z., Bélanger, S., Larouche, P., 2012. Evaluation of ocean color algorithms in the southeastern Beaufort Sea, Canadian Arctic: New parameterization using SeaWiFS, MODIS, and MERIS spectral bands. Can. J. Remote Sensing 38 (5), 535–556. https://doi.org/10.5589/m12-045.

Blais, M., Ardyna, M., Gosselin, M., Dumont, D., Bélanger, S., Tremblay, J.-É., Gratton, Y., Marchese, C., Poulin, M., 2017. Contrasting interannual changes in phytoplankton productivity and community structure in the coastal Canadian Arctic Ocean. Limnol. Oceanogr. 62, 2480–2497. https://doi.org/10.1002/lno.10581.

Brewin, R.J.W., Sathyendranath, S., Müller, D., Brockmann, C., Deschamps, P.Y., Devred, E., Doerffer, R., Fomferra, N., Franz, B., Grant, M., Groom, S., Horseman, A., Hu, C., Krasemann, H., Lee, Z.P., Maritorena, S., Mélin, F., Peters, M., Platt, T., Regner, P., Smyth, T., Steinmetz, F., Swinton, J., Werdell, J., White, G.N., 2015. The ocean colour climate change initiative: III. A round-robin comparison on in-water bio-optical algorithms. Remote Sens. Environ. 162, 271–294. https://doi.org/10.1016/j.rse.2013.09.016.

Bricaud, A., Morel, A.Y., 1987. Atmospheric corrections and interpretation of marine radiances in CZCS imagery: use of a reflectance model. Oceanol. Acta 7 (2), 53–62.

Campbell, J.W., 1995. The lognormal distribution as a model for bio-optical variability in the sea. J. Geophys. Res. 100, 12237–13254. https://doi.org/10.1029/95JC00458.

Carmack, E, Wassmann P., 2006. Food webs and physical–biological coupling on pan-Arctic shelves: unifying concepts and comprehensive perspectives. Progress in Oceanography 71 (2–4), 446–477. https://doi.org/10.1016/j.pocean.2006.10.004.

Cavalieri, D.J., Parkinson, C.L., Gloersen, P., Zwally, H.J., 1996. updated yearly. Sea Ice Concentrations from Nimbus-7 SMMR and DMSP SSM/I-SSMIS Passive Microwave Data, Version 1 [daily, Arctic Ocean, 1978–2015]. Natl. Snow Ice Data Center, Boulder, Color. USA. https://doi.org/10.5067/8GQ8LZQVL0VL.

Dee, D.P., Uppala, S.M., Simmons, A.J., Berrisford, P., Poli, P., Kobayashi, S., Andrae, U., Balmaseda, M.A., Balsamo, G., Bauer, P., Bechtold, P., Beljaars, A.C.M., van de Berg, L., Bidlot, J., Bormann, N., Delsol, C., Dragani, R., Fuentes, M., Geer, A.J., Haimberger, L., Healy, S.B., Hersbach, H., Hólm, E.V., Isaksen, L., Kållberg, P., Köhler, M., Matricardi, M., Mcnally, A.P., Monge-Sanz, B.M., Morcrette, J.J., Park, B. K., Peubey, C., de Rosnay, P., Tavolato, C., Thépaut, J.N., Vitart, F., 2011. The ERA-interim reanalysis: configuration and performance of the data assimilation system. Q. J. R. Meteorol. Soc. 137, 553–597. https://doi.org/10.1002/qj.828.

Djavidnia, S., Mélin, F., Hoepffner, N., 2010. Comparison of global ocean colour data records. Ocean Sci. 6, 61–76. https://doi.org/10.5194/os-6-61-2010.

Eplee, R.E., Patt, F.S., Barnes, R.A., McClain, C.R., 2007. SeaWiFS long-term solar diffuser reflectance and sensor noise analyses. Appl. Opt. 46, 762–773. https://doi.org/10.1364/AO.46.000762.

Evans, R.H., Gordon, H.R., 1994. Coastal zone color scanner “system calibration”: a retrospective examination. J. Geophys. Res. 99, 7293–7307.

Evers-King, H., Martinez-Vicente, V., Brewin, R.J.W., Dall’Olmo, G., Hickman, A.E., Jackson, T., Kostadinov, T.S., Krasemann, H., Loisel, H., Röttgers, R., Roy, S., Stramski, D., Thomalla, S., Platt, T., Sathyendranath, S., 2017. Validation and intercomparison of ocean color algorithms for estimating particulate organic carbon in the oceans. Front. Mar. Sci. 4, 1–20. https://doi.org/10.3389/fmars.2017.00251.

Fossheim, M., Primicerio, R., Johannesen, E., et al., 2015. Recent warming leads to a rapid borealization of fish communities in the Arctic. Nat. Clim. Chang. 5, 673–677.

Franz, B.A., Bailey, S.W., Werdell, P.J., McClain, C.R., 2007. Sensor-independent approach to the vicarious calibration of satellite ocean color radiometry. Appl. Opt. 46, 5068–5082. https://doi.org/10.1364/AO.46.005068.

Granskog, M.A., Macdonald, R.W., Mundy, C.-J., Barber, D.G., 2007. Distribution, characteristics and potential impacts of chromo- phoric dissolved organic matter (CDOM) in Hudson Strait and Hudson Bay, Canada. Continent. ShelfRes. 27 (15), 2032–2050. https://doi.org/10.1016/j.csr.2007.05.001.

Gravetter, F., Wallnau, L, 2014. Essentials of statistics for the behavioral sciences. Cengaged Learning, Wadsworth (8th Edition).

Gregg, W.W., Conkright, M.E., 2002. Decadal changes in global ocean chlorophyll. Geophys. Res. Lett. 29 https://doi.org/10.1029/2002GL014689.
Gregg, W.W., Rousseaux, C.S., 2014. Decadal trends in global pelagic ocean chlorophyll: a new assessment integrating multiple satellites, in situ data, and models. J. Geophys. Res. Ocean. 119, 5921–5933. https://doi.org/10.1002/2014JC010158.
Henson, S.A., Beaulieu, C., Lampitt, R., 2016. Observing climate change trends in ocean biogeochemistry: when and where. Glob. Chang. Biol. 22, 1561–1571. https://doi.org/10.1111/gcb.13152.
Hill, V., Ardyna, M., Lee, S.H., Varela, D.E., 2018. Decadal trends in phytoplankton production in the Pacific Arctic Region from 1950 to 2012. Deep-Sea Res. II 152, 82–94.
Hooker, S.B., Esaias, W.E., 1993. An overview of the SeaWiFS project. EOS Trans. Am. Geophys. Union 74, 241–246. https://doi.org/10.1029/93EO00945.
Hoppe, C.J.M., Wolf, K.K.E., Schuback, N., Tortell, P.D., Rost, B., 2018. Compensation of ocean acidification effects in Arctic phytoplankton assemblages. Nat. Clim. Chang. 8, 529–533. https://doi.org/10.1038/s41558-018-0142-9.
Kahru, M., Brotas, V., Manzano-Sarabia, M., Mitchell, B.G., 2011. Are phytoplankton blooms occurring earlier in the Arctic? Glob. Chang. Biol. 17, 1733–1739. https://doi.org/10.1111/j.1365-2486.2010.02312.x.
Kinney, C.J., Maslowski, W., Osinski, R., Jin, M., Frants, M., Jeffery, N., et al., 2020. Hidden production: on the importance of pelagic phytoplankton blooms beneath Arctic Sea ice. J. Geophys. Res. Oceans 125 e2020JC016211.
Kohlbach, D., Graeve, M.A., Lange, B., David, C., Peeken, I., Flores, H., 2016. The importance of ice algae-produced carbon in the Central Arctic Ocean ecosystem: food web relationships revealed by lipid and stable isotope analyses. Limnol. Oceanogr. 61, 2027–2044. https://doi.org/10.1002/lno.10351.
Kwok, R., 2018. Arctic Sea ice thickness, volume, and multiyear ice coverage: losses and coupled variability (1958-2018). Environ. Res. Lett. 13 https://doi.org/10.1088/1748-9326/aae3ec.
Lalande, C., Nöthig, E.-M., Somavilla, R., Bauerfeind, E., Shevchenko, V., Okolodkov, Y., 2014. Variability in under-ice export fluxes of biogenic matter in the Arctic Ocean. Glob. Biogeochem. Cycles 28, 571–583. https://doi.org/10.1002/2013GB004735.
Lee, Y.J., Matrai, P.A., Friedrichs, M.A.M., Saba, V.S., Antoine, D., Ardyna, M., Asanuma, I., Babin, M., Bélanger, S., Benoît-Gagné, M., Devred, E., Fernández-Méndez, M., Gentili, B., Hirawake, T., Kang, S.H., Kameda, T., Katlein, C., Lee, S.H., Lee, Z., Mélin, F., Scardi, M., Smyth, T.J., Tang, S., Turpie, K.R., Waters, K.J., Westberry, T.K., 2015. An assessment of phytoplankton primary productivity in the Arctic Ocean from satellite ocean color/in situ chlorophyll-a based models. J. Geophys. Res. Ocean. 120, 6508–6541. https://doi.org/10.1002/2015JC011018.
Lewis, K.M., Arrigo, K.R., 2020. Ocean color algorithms for estimating chlorophyll a, CDOM absorption, and particle backscattering in the Arctic Ocean. J. Geophys. Res. Ocean. 125, 1–23. https://doi.org/10.1029/2019JC015706.
Lewis, K.M., Van Dijken, G.L., Arrigo, K.R., 2020. Changes in phytoplankton concentration now drive increased Arctic Ocean primary production. Science (80-.) 369, 198–202. https://doi.org/10.1126/science.aay8380.
Longhurst, A.R., 1981. Analysis of Marine Ecosystems, First edition. Acad. Press London. https://doi.org/10.1016/0044-8486(83)90244-2.
Longhurst, A.R., 2007. Toward an ecological geography of the sea. Ecol. Geogr. Sea 1–17. https://doi.org/10.1016/b978-012455521-1/50002-4.
Longhurst, A., Sathyendranath, S., Platt, T., Caverhill, C., 1995. An estimate of global primary production in the ocean from satellite radiometer data. J. Plankton Res. 17, 1245–1271. https://doi.org/10.1093/plankt/17.6.1245.
Mäkelä, A., Witte, U., Archambault, P., 2017. Ice algae versus phytoplankton: resource utilization by Arctic deep sea macroinfauna revealed through isotope labelling experiments. Mar. Ecol. Prog. Ser. 572, 1–18. https://doi.org/10.3354/meps12157.
Maritorena, S., Siegel, D.A., 2005. Consistent merging of satellite ocean color data sets using a bio-optical model. Remote Sens. Environ. 94, 429–440. https://doi.org/10.1016/j.rse.2004.08.014.
Maritorena, S., Siegel, D.A., Peterson, A.R., 2002. Optimization of a semianalytical ocean color model for global-scale applications. Appl. Opt. 41, 2705. https://doi.org/10.1364/ao.41.002705.
Martinez, E., Antoine, D., D'Ortenzio, F., Gentili, B., 2009. Climate-driven basin-scale decadal oscillations of oceanic phytoplankton. Science (80-.) 326, 1253–1256. https://doi.org/10.1126/science.1177012.
Matsuoka, A., Bricaud, A., Benner, R., Para, J., Sempéré, R., Prieur, L., Bélanger, S., Babin, M., 2012. Tracing the transport of colored dissolved organic matter in water masses of the Southern Beaufort Sea: relationship with hydrographic characteristics. Biogeosciences 9, 925–940. https://doi.org/10.5194/bg-9-925-2012.
McClain, C.R., 2009. A decade of satellite ocean color observations. Annu. Rev. Mar. Sci. 1, 19–42. https://doi.org/10.1146/annurev.marine.010908.163650.
McClain, C.R., Hooker, S., Feldman, G., Bontempi, P., 2006. Satellite data for ocean biology, biogeochemistry, and climate research. Eos (Washington. DC) 87, 340–342. https://doi.org/10.1029/2006eo340002.
Meister, G., Franz, B.A., 2014. Corrections to the MODIS aqua calibration derived from MODIS Aqua Ocean color products. IEEE Trans. Geosci. Remote Sens. 52, 6534–6541. https://doi.org/10.1109/TGRS.2013.2297233.
Melin, F., 2010. Global distribution of the random uncertainty associated with satellite-derived Chl a. IEEE Geosci. Remote Sens. Lett. 7, 220–224. https://doi.org/10.1109/LGRS.2009.2031825.
Mélin, F., Chuprin, A., Grant, M., Jackson, T., Swinton, J., Sathyendranath, S., 2016. Ocean Colour Climate Change Initiative (OC-CCI) – Phase Two, Ocean Colour Data Bias Correction and Merging. Tech. Rep., Plymouth Marine Laboratory.
Mitchell, B.G., 1992. Predictive bio-optical relationships for polar oceans and marginal ice zones. J. Mar. Syst. 3, 91–105. https://doi.org/10.1016/0924-7963(92)90032-4.
Mitchell, B.G., 1994. Coastal zone color scanner retrospective. J. Geophys. Res. 99, 7291. https://doi.org/10.1029/93JC03259.
Moigne, F.A.C., Poulton, A.J., Henson, S.A., Daniels, C.J., Fragoso, G.M., Mitchell, E., Richier, S., Russell, B.C., Smith, H.E.K., Tarling, G.A., Young, J.R., Zubkov, M., 2015. Carbon export efficiency and phytoplankton community composition in the Atlantic sector of the Arctic Ocean. J. Geophys. Res. Ocean. 120, 3896–3912. https://doi.org/10.1002/2015JC010700.
Morel, A., Maritorena, S., 2001. Bio-optical properties of oceanic waters: a reappraisal. J. Geophys. Res. Ocean. 106, 7163–7180. https://doi.org/10.1029/2000jc000319.
Oziel, L., Neukermans, G., Ardyna, M., Lancelot, C., Tison, J.-L.J.-L., Wassmann, P., Sirven, J., Ruiz-Pino, D., Gascard, J.-C.J.-C., 2017. Role for Atlantic inflows and sea ice loss on shifting phytoplankton blooms in the Barents Sea. J. Geophys. Res. Ocean. 122, 5121–5139. https://doi.org/10.1002/2016JC012582.
Nöthig, E.-M., Ramondenc, S., Haas, A., Hehemann, L., Walter, A., Bracher, A., et al., 2020. Summertime in situ chlorophyll a and particulate organic carbon standing stocks in surface waters of the Fram Strait and the Arctic Ocean (1991–2015). Front. Mar. Sci. 7 (350).
Oziel, L., Massicotte, P., Babin, M., Devred, E., 2022. Decadal changes in Arctic Ocean Chlorophyll a: bridging ocean color observations from the 1980s to present time. SEANOE. https://doi.org/10.17882/86601.
Peng, G., Meier, W.N., 2018. Temporal and regional variability of Arctic sea-ice coverage from satellite data. Ann. Glaciol. 59, 191–200. https://doi.org/10.1017/aog.2017.32.
Racault, M.F., Sathyendranath, S., Platt, T., 2014. Impact of missing data on the estimation of ecological indicators from satellite ocean-colour time-series. Remote Sens. Environ. 152, 15–28. https://doi.org/10.1016/j.rse.2014.05.016.
Renaut, S., Devred, E., Babin, M., 2018. Northward expansion and intensification of phytoplankton growth during the early ice-free season in Arctic. Geophys. Res. Lett. 45, 10,590–10,598. https://doi.org/10.1029/2018GL078995.
Sathyendranath, S., Brewin, R.J.W., Brockmann, C., Brotas, V., Calton, B., Chuprin, A., Cipollini, P., Couto, A.B., Dingle, J., Doerffer, R., Donlon, C., Dowell, M., Farman, A., Grant, M., Groom, S., Horseman, A., Jackson, T., Krasemann, H., Lavender, S., Martinez-Vicente, V., Mazeran, C., Mélin, F., Moore, T.S., Müller, D., Regner, P., Roy, S., Steele, C.J., Steinmetz, F., Swinton, J., Taberner, M., Thompson, A., Valente, A., Zühlke, M., Brando, V.E., Feng, H., Feldman, G., Franz, B.A., Frouin, R., Gould, R.W., Hooker, S.B., Kahru, M., Kratzer, S., Mitchell, B.G., Muller-Karger, F.E., Sosik, H.M., Voss, K.J., Werdell, J., Platt, T., 2019. An ocean-colour time series for use in climate studies: the experience of the ocean-colour climate change initiative (OC-CCI). Sensors (Switzerland) 19. https://doi.org/10.3390/s19194285.
Serreze, M.C., Meier, W.N., 2019. The Arctic's sea ice cover: trends, variability, predictability, and comparisons to the Antarctic. Ann. N. Y. Acad. Sci. 1436, 36–53. https://doi.org/10.1111/nyas.13856.
Slagstad, D., Wassmann, P.F.J., Ellingsen, I., 2015. Physical constrains and productivity in the future Arctic Ocean. Front. Mar. Sci. 2, 1–23. https://doi.org/10.3389/fmars.2015.00085.
Spalding, M.D., Agostini, V.N., Rice, J., Grant, S.M., 2012. Pelagic provinces of the world: A biogeographic classification of the world's surface pelagic waters. https://doi.org/10.1016/j.ocecoaman.2011.12.016.
Stroeve, J., Notz, D., 2018. Changing state of Arctic Sea ice across all seasons. Environ. Res. Lett. 13, 103001 https://doi.org/10.1088/1748-9326/aade56.
Stumpf, R.P., Gould, R.W., Martilomich, O.M., Ransibrahmanakul, V., 2003. Algorithm Updates for the Fourth SeaWiFS Data Reprocessing.
Tremblay, J.-E., Robert, D., Varela, D.E., Lovejoy, C., Darnis, G., Nelson, R.J., Sastri, A.R., 2012. Current state and trends in Canadian Arctic marine ecosystems: I. Primary production, Climatic Change 115, 161–178. https://doi.org/10.1007/s10584-012-0496-3.
Vancoppenolle, M., Bopp, L., Madec, G., Dunne, J., Ilyina, T., Halloran, P.R., et al., 2013. Future arctic ocean primary productivity from CMIP5 simulations: uncertain outcome, but consistent mechanisms. Glob. Biogeochem. Cycles 27, 605–619.
Werdell Jeremy, P., B. Franz, S. Bailey, G. Feldman, E. Boss, V. Brando, et al., 2013. Generalized ocean color inversion model for retrieving marine inherent optical properties. Applied Optics 54 (10), 2019–2037. https://doi.org/10.1364/ao.52.002019.
Werdell, P.J., Bailey, S.W., Franz, B.A., Morel, A., McClain, C.R., 2007. On-orbit vicarious calibration of ocean color sensors using an ocean surface reflectance model. Appl. Opt. 46, 5649–5666. https://doi.org/10.1364/AO.46.005649.